Kinetics of Ethylene Glycol: The first validated reaction scheme and first measurements of ignition delay times and speciation data

Trupti Kathrotia*, Clemens Naumann, Patrick Oßwald, Markus Köhler, Uwe Riedel

Combustion and Flame, 179, (2017) pp. 172-184

The original publication is available at www.elsevier.com

http://dx.doi.org/10.1016/j.combustflame.2017.01.018

Kinetics of Ethylene Glycol: The first validated reaction scheme and first measurements of ignition delay times and speciation data

Trupti Kathrotia*, Clemens Naumann, Patrick Oßwald, Markus Köhler, Uwe Riedel

Institute of Combustion Technology, German Aerospace Center (DLR), Pfaffenwaldring 38-40, D-70569 Stuttgart, Germany

*Corresponding author: Trupti Kathrotia

German Aerospace Center *(DLR)*

Pfaffenwaldring 38-40

D-70569 Stuttgart

Germany

Email: trupti.kathrotia@dlr.de

Abstract

The reaction kinetics of Ethylene Glycol (EG) is studied, due to its similarity in chemical composition and physical properties, as a model fuel for pyrolysis oil. Recently, the combination of fast pyrolysis of residual biomass and subsequent gasification of the pyrolysis oil has gained high interest. In the gasification process, oxygen is often used as a gasifying agent (e.g. auto-thermal gasification) which led us to study EG under oxidation condition.

This study has experimental and modeling objectives: We obtain novel experimental data that we use for validation of our EG oxidation model that enable predictive modeling and optimization of gasifiers through multi-dimensional CFD simulations. Both, detailed and reduced skeletal models are obtained. The validation data needed for the model is studied in two different types of experiments namely, (1) ignition delay times obtained behind reflected shock waves in the temperature range of 800 – 1500 K at 16 bar and, (2) quantitative species profiles measured in a high temperature flow reactor setup for fuel equivalence ratios Φ = 1.0 and 2.0 in the temperature range of 700 – 1200 K. Both experiments are performed in the EG-system for the first time providing the relevant basis for the understanding on how EG decomposes and for the optimization of the reaction mechanism. The influence of different product channels on the reactivity of the EG system is investigated and leads us to pose the question, if enol can be formed in this combustion (oxidative) environment.

Keywords: Ethylene glycol, gasification, ignition delay times, flow reactor, detailed reaction mechanism, reduced mechanism

1. Introduction

Reaching for renewable alternative energy sources, fuels that are carbon neutral and ensure security of supply at affordable price are of high interest in the energy sector including the biomass-based fuels. In the EU, the current target of 20% final energy consumption from renewable sources by 2020 is already closing its goal with 15.3% projected in 2014. A renewed target is set to 27% by 2030 [1]. These targets are also part of the EU's energy and climate goals for 2030. Though the biomass based resources are renewable, their rate of regeneration is low. Therefore, to achieve maximum use, more efficient processes to convert biomass are required.

Energy densification is the major motivation behind the conversion of biomass to liquid fuels. As an example from Kolb et al. [2], a dry biomass with an energy density of 2 MJ/L can be converted by gasification to a syngas of 25 MJ/L. Through Fischer Tropsch (FT) processing, produced fuels features energy densities of approximately 36 MJ/L. Gasification of the pyrolysis oil is not strictly a pyrolysis process. Especially, entrained flow gasification, which is often used in large scale devices, is an oxidative environment [3]. In auto-thermal gasifiers oxygen (or air) is often employed as a gasifying agent to supply heat to drive the overall endothermic process. Insertion of the gasifying agent depends on the type of gasifier used (in fluidized bed in 2nd phase after pyrolysis; in entrained-flow gasifiers in single stage at the start). In addition, understanding the reaction kinetics at a wide range of fuel stoichiometry is important as it has influence on the gasification efficiency and carbon conversion. The change in fuel stoichiometry would move the gasification to combustion thereby changing the product spectrum. Therefore, the focus of our work is on the oxidation of ethylene glycol (EG) including stoichiometric and rich conditions.

The pyrolysis oil entering a gasifier typically contains high amount of oxygen due to a variety of oxygen containing heteropolymer present in the original feedstock. The process occurring inside

the gasifier is complex and involves multiphase chemistry. For computational fluid dynamics (CFD) study of a gasifier, one needs a reaction kinetic model. To this end, EG is selected as a model fuel for pyrolysis oil [3,4] based on its similarity in the chemical composition and physical properties. The unusual high content of oxygen (30–60 wt%) in pyrolysis oil is matched by the two oxygen atoms present in the EG molecule. In addition to reasons on safety and price, EG is a single component surrogate providing a striking advantage for the reaction model development and also in terms of computational resources needed to perform CFD calculations.

The presented model is based on our previous work: a model of EG published by Hafner et al. [5,6]. This model, however, has not been sufficiently validated due to the lack of experimental data at the given time. At first, a revision of this mechanism was required mainly to reduce numerical stiffness. Due to the lack of any experiments in combustion environment, understanding of EG combustion chemistry was impossible. Therefore, a new set of validation experiments have been undertaken in the present work which has improved the previous understanding of the decomposition routes of EG.

This study provides an important reaction chemistry model for the computational gasification studies. The high temperature shock-tube experiments are performed for stoichiometric mixtures diluted in argon and at pressure of 16 bar. The atmospheric flow reactor measurements at intermediate temperature range and at two stoichiometries (Φ = 1.0 and 2.0) provide the spectrum of intermediates and products formed during the oxidation process. These are used to validate the reaction model and understand the underlying chemistry of EG oxidation. A detailed comparison of fuel intermediates and their formation paths is described in the present work. In addition, a reduced skeletal mechanism is also presented comprising 43 species and 270

reactions to be used to speed up multi-dimensional CFD calculations (the Supplemental Material provides additional information on the reduced model validation). Thus this work presents the first validated reaction mechanism based on the first experimental investigations of ignition delay times and species profiles measured in a shock-tube and a flow reactor environment, respectively.

1.1 Ethylene Glycol – Selection as pyrolysis oil surrogate

The biomass feedstock is converted to the pyrolysis oil prior to gasification. This pyrolysis oil, also referred as bio-syncrude oil, or simply bio-oil, is highly oxygenated and is highly viscose at ambient conditions. It possesses poor stability due to its high intrinsic oxygen content, usually 30 to 60 wt% [7,8], depending on the feedstock. This high oxygen content in pyrolysis oil stems from heteropolymers lignin, cellulose and hemicellulose present in the feed stock.

The selection of EG is based on its similar physical-chemical characteristics to the pyrolysis oil obtained from varying feedstocks. Typical physical properties and chemical composition of the pyrolysis oil obtained from different literature sources are summarized in Table 1. These properties vary by the extraction methods used and by the type of biomass from which they are extracted. Table 1 also shows the properties of EG for a direct comparison and for its apparent selection and suitability as a pyrolysis oil surrogate.

Table 1: Comparison of physical properties and chemical composition of pyrolysis oil obtained from different feedstock and EG.

Properties / Bio-oil	Density (kg/m^3)	Dynamic Viscosity (cP)	Pour point (°C)	Flash point (°C)	Enthalpy of combustion ($MJ \cdot kg^{-1}$)	Acidity pH	H_2O Content (wt%)	Composition (wt%)		
								C	H	O
Ethylene glycol [9]	1132 (20°C)	18–56 (0–24°C)	-12	111	16.96	-	-	38.7	9.7	51.6
BTG-BtL	1170	20–100 (50°C)	-	-	16–19	2.9	15–35	46	7	47
Pyrolysis oil [10]	1100–1300	40–100	-36 – -9	45–100	16–19	2.0–3.5	15–30	32–49	6–8	44–60
Bio-oil [11]	1250 (20°C)	-	-	-	17.51	2.0–3.8	15–30	60.6	7.7	29.2
Bio-oil [12]	-	-	-	-	-	-	10–30	47.5–56.8	7.0–8.5	31.3–45.2
From various feedstock [8]	-	-	-36 – -9	50–100	13–18	2.0–3.7	15–30	32–49	6.9–8.6	44–60
ASTM7544 [13]	1100–1300 (20°C)	-	-9	>45	>15	-	<30	-	-	-

The enthalpy of combustion of most hydrocarbon fuel ranges from 41 – 44 $MJ \cdot kg^{-1}$ which is about twice as high as the heat obtained from the biomass combustion (about 13 – 18 $MJ \cdot kg^{-1}$). The enthalpy of combustion of EG is about 17 $MJ \cdot kg^{-1}$ making it suitable surrogate fuel for pyrolysis oil. In addition, the chemical composition of the pyrolysis oil depending on the source of the feedstock varies from 32–60 (wt%) carbon, 7–10 (wt%) hydrogen, and 30–60 (wt%) oxygen. The chemical composition of EG lies within this typical range. Similarly, liquid properties such as the density or the viscosity of EG are comparable to the properties of the pyrolysis oil. Thus, this comparison justifies the selection of EG as a suitable surrogate for the pyrolysis oil.

1.2 Ethylene Glycol – Reaction kinetics

The molecule EG contains two hydroxyl groups attached to the ethane molecule and it is similar to ethanol (one less hydroxyl group). Therefore it is reasonable to assume that the decomposition of EG is similar to ethanol. The theoretical studies of Park et al. [14] showed that water elimination is the major path in ethanol decomposition ($C_2H_5OH \rightarrow C_2H_4 + H_2O$) with a 66.6 kcal·mol^{-1} barrier. The only information available on the thermal decomposition of EG over a wide temperature and pressure range is a theoretical study from Ye et al. [15]. Based on their theoretical analysis they predicted that the water elimination from the EG molecule ($EG \rightarrow C_2H_4O + H_2O$) also has the lowest energy barrier and is about 3.7 kcal·mol^{-1} higher than that of ethanol. The decomposition of ethanol forms ethane in the H_2O elimination path ($C_2H_5OH \rightarrow C_2H_4 + H_2O$) whereas EG would form C_2H_4O ($EG \rightarrow C_2H_4O + H_2O$). Unlike ethanol, where the ethenol formation through H_2 elimination ($C_2H_5OH \rightarrow CH_2CHOH + H_2$) has a much higher energy barrier (106.3 kcal·mol^{-1}) [14], EG ($EG \rightarrow CH_2CHOH + H_2O$) in comparison only has a 70.3 kcal·mol^{-1} barrier. Among C_2H_4O isomers either acetaldehyde or ethenol or both can be formed. Ye and coworkers [15] predicted the energy difference between enol (ethenol) and aldehyde (acetaldehyde) formation to be only 0.9 kcal·mol^{-1} and thereby the possibility of both reaction routes ($EG \rightarrow CH_2CHOH/CH_3CHO + H_2O$), with enol as the more favored route. Thus, EG studies with respect to major decomposition product C_2H_4O differ from ethanol. Though acetaldehyde is part of most reaction mechanisms, the presence of ethenol is often restricted. Since ethenol is a direct decomposition product of EG we believe in its crucial importance.

The role of ethenol itself in the combustion chemistry is discussed since its first detection in hydrocarbon flames by photoionization mass spectrometry using synchrotron radiation [16]. Since most of the *in situ* mass spectrometry experiments performed in the combustion

environment only identify overall m/z and not the molecular structure, there are limited reports on any direct evidence of the presence of ethenol in combustion or gasification.

To understand the role of ethenol in combustion requires addressing two aspects: Namely, its formation as well as its removal reactions. Compared to ethenol, acetaldehyde is considered more stable at any temperatures. Taatjes et al. [17,18] investigated many hydrocarbon flames depicting most of the chemical classes and concluded that in the low pressure hydrocarbon flames, the major source of enols is through reactions of alkenes with OH. Since then, various studies reported ethenol formation in hydrocarbons and various oxygenated fuels [14,19-26]. The consumption of ethenol can be through direct and/or radical-catalyzed tautomerization forming acetaldehyde or through decomposition forming other products. There are many investigations in the literature [16,19] stating that despite the thermal stability of acetaldehyde, the ethenol to acetaldehyde via direct tautomerization reaction (which requires 1-3 hydrogen migration) has a high energy barrier and therefore major ethenol consumption would be not be favored via this route. Li et al. [26] observed that the position of hydroxyl group on parent hydrocarbon plays an important role on how enols are formed.

Based on the information on the energy barriers from the literature studies, pointing to the possibility of enols in combustion, we expect that ethenol is formed in the EG oxidation. It may quickly isomerized/tautomerized to acetaldehyde and therefore the equilibrium concentration may not show any ethenol. This will also depend on the system studied. For example, it is more likely that isomerization reactions which are important at low temperatures are more feasible in the flow reactor studies where the reactor temperature is raised slowly whereas in the shock-tube experiments the rapid rise in the temperature will rather allow a rapid decomposition process to be dominant. However, our currents experiments are not sufficient to distinguish and confirm if

ethenol or acetaldehyde is the major product of EG decomposition in the water elimination reactions. Therefore, we consider only acetaldehyde that is already part of C_1-C_2 hydrocarbon mechanism as a lumped C_2H_4O species to be the direct decomposition product of EG. Advanced experiments like iPEPICO [27], PIMS [28] or theoretical studies are needed in the future to provide more knowledge on the role of ethenol in EG oxidation.

2. Experimental method

The purpose of the experiments conducted below is two-fold. Firstly, for purely validation purpose where stoichiometric conditions (shock-tube, flow reactor) are selected as a starting point to understand the reaction kinetics of EG whereas fuel-rich chemistry (flow reactor) is studied for understanding of complex reaction kinetics arising from the recombination of methyl radicals.

2.1 Shock-tube

The ignition delay time experiments were carried out in a high pressure shock-tube with an internal diameter of 46 mm. For the schematic and detailed description of the shock-tube setup we divert readers to the Supplemental material. The shock-tube is divided by aluminium diaphragms into a driver section of 10.08 m and a driven section of 3.25 m in length. The driver section is heated to 120 °C. It is filled using two Bronkhorst® mass flow controllers. Helium was used as the main component, and Ar was added to match the acoustic impedance of the driver gas. These tailored conditions allowed to extend measurement times [29]. The driven section is heated to 180 °C and is pumped down to pressures $p < 10^{-4}$ mbar by a turbo-molecular pump. Gas mixtures were prepared manometrically in a 8.4 l stainless steel vessel, which was heated to

200 °C, nitrogen flushed and evacuated using a rotary vane pump and liquid nitrogen cooled trap to pressures below 10^{-2} mbar. For each experiment a new mixture is prepared by injecting the EG with a syringe in a small, glass fibre stuffed pre-volume. The syringe is weighed before and after the injection with an accuracy of ±3mg@260g (Ohaus AV264). Preheated nitrogen transports the evaporated fuel into the evacuated vessel where it is mixed with synthetic air (80 vol% N_2, 20 vol% O_2) afterwards. After stirring the mixture with a paddle for 15 min the EG/synthetic air/N_2 mixture is filled into the shock-tube. The compositions of the mixtures were controlled by gas chromatographic analysis at random sampling (SHIMADZU GC-2010 with FID (Flame Ionization Detector) and Zebron wax column, 1-Pentanol as internal standard and acetone as solvent). The EG loss due to the washing-out with acetone was determined to be 2%. Mixtures in the nitrogen testing EG pyrolysis yielded nearly complete recovery rates. Probes of ignitable mixtures were taken directly from the mixing vessel as well as from the shock-tube at a port close to the end flange. The EG recovery rates from the shock-tube were determined to be 77(±12) %, whereas 91(±5) % could be recovered from the mixing vessel after a mixing time of 15 min. compromising mixture homogeneity and fuel degradation. The fuel degradation products were not identified.

The incident shock wave velocity was measured over four 30 mm intervals in the measurement section using five piezo-electric pressure gauges. The temperature and pressure behind the reflected shock wave were computed from the measured incident shock speed and the attenuation using a one-dimensional shock model.

The ignition was observed by measuring pressure profiles (Figure 1) with piezoelectric gauges (PCB® 112A05 and Kistler® 603B) located in a measurement plane at a distance of 10 mm to the end flange. Both pressure gauges were protected by a 1 mm high temperature silicon rubber

shield (RTV 116) to reduce heat transfer and thus signal drift. A third unshielded piezoelectric gauge (Kistler® 603B) in the same measurement plane revealed this time-dependent signal drift. Also, the CH* chemiluminescence at 431 nm at the same position was selected by narrow band pass filters (FWHM = 5 nm), measured with a photomultiplier (HAMAMATSU R3896) and amplified by a logarithmic amplifier (FEMTO HLVA-100), mapping an input signal of four orders of magnitude to an output signal range of 0 – 1 V. All ignition delay time values shown in this paper were determined by measuring the time difference between the initiation of the system by the reflected shock wave and the occurrence of the first CH* maximum at the radial port, because this allows a good comparability to the simulations (Figure 1).

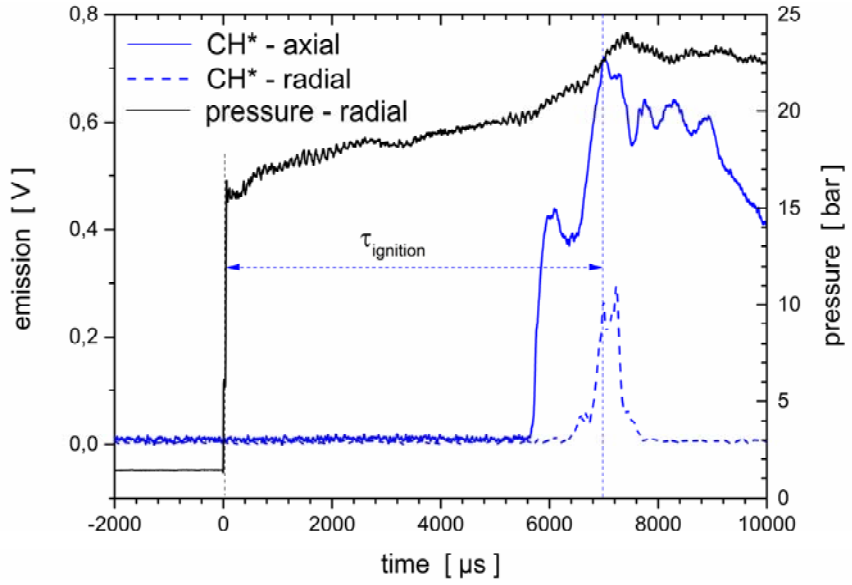

Figure 1: Emission and pressure profiles of EG / synthetic air / N_2 mixture at $\Phi_{nominal} = 1$, initial T = 880 K and p = 15.2 bar at a dilution in N_2 of 1:2.

In addition, the CH* emission has been detected through the end-plate window and by two additional ports further downstream to monitor the emission due to the propagation of the deflagration wave (not shown). The temporal difference in the CH* profiles between the axial and the radial detection can be explained by the dynamic of the ignition process. The axial

detector with an unrestricted field of view detected emission at 431 nm occurring anywhere in the tube. The radial detectors have a restricted Field of View (FOV) to enhance the spatial resolution. The interpretation of the emission profiles and their temporal evolution can be explained by the dynamical development of the ignition: Firstly, the ignition proceeds are locally restricted, i.e. between end plate and radial measurement plane, giving rise to the first light. Secondly, as shown in the Figure 1, a typical dip in the endplate's emission records is observed, more or less pronounced, which is associated with a first detection of light at the radial port. The "mobilization" of the ignition, i.e. the generation of a flame front or deflagration, shortly enhances the radiation less deactivation of excited species, before it is accelerating. Following the direction and the propagation velocity of the deflagration via the timely shifted CH* emission at the two ports further downstream supports this explanation.

The experimental setup allows measurements of ignition delay times for observation periods up to 30 ms depending on the temperature. Nevertheless, post shock compression due to attenuation of reflected shock front imposes a dynamic pressure profile, increasing the pressure by about 20% after 9 ms in mixtures that have not yet released heat. This facility dependent effect was taken into account assuming adiabatic isentropic compression when modeling the data.

2.2 Flow reactor

Species profiles are measured using the DLR high temperature flow reactor setup. The system, including the flow reactor and the molecular beam mass spectrometric (MBMS) in situ detection is described in detail elsewhere [30] and thus only brief descriptions are given here and the schematic is provided in the Supplemental Material.

The flow reactor consists of a 40 mm inner diameter ceramic (Al_2O_3) pipe of 1497 mm length placed in a high temperature oven (Gero, Type HTRH 40-1000) providing a total heated section of 1000 mm in length. Note that the length of the reaction segment is not subject to thermal expansion. Gases are fed premixed and vaporized into the reactor by a tempered flange (80°C). The highly diluted (ca. 99 vol% in Ar), laminar flowing reactant mixture passes through a known temperature profile (details on temperature characterization will be given below). Detection of the gas composition takes place at the reactor outlet as a function of the oven temperature. Measurements are performed at constant inlet mass flow, while a monotonically decreasing temperature ramp (-200 K/h) is applied to the oven in the range of 1350 K to 670 K. The temperature ramp is selected as compromise of averaging time for a (negligible) small temperature increment and total measurement time per series. Note that identical profiles may be obtained when distinct temperatures are measured at isotherm oven temperatures (when thermal inertia is considered properly). Thus averaging time of the MBMS corresponds to 2.5 K. The corresponding residence times are around 2 s (1000 K) for the given conditions. Changes in the flow velocity and thus the residence time are considered in the model calculations by the application of the respective temperature profile.

All input streams are metered in high precision by Coriolis mass flow meters (Bronkhorst, Mini Cori-Flow M12, M13 and M14). Vaporization for the EG is realized by a commercial vaporizer system (Bronkhorst, CEM) at 150 °C; conditions are chosen and found to prevent condensation in the heated supply lines (130 °C) as well as thermal decomposition of the fuel. For the present study, we have investigated rich (Φ = 2.0) and stoichiometric (Φ = 1.0) conditions at constant carbon flux, the specific flowrates are: 17.6 g/min Ar (9.9 slm), 69.2 mg/min EG and 89.2

mg/min (Φ = 1.0) or 44.6 mg/min (Φ = 2.0) O_2, respectively. The total volume flow is close to 10 slm.

Gases are withdrawn by a quartz cone at the centerline of the reactor exit at ambient pressures (around 960 mbar corresponding to 550 m above sea level). Sampling is centered at the end of the reaction zone, roughly 30 mm within the reactor exit via a 50 µm orifice at the quartz nozzle tip. The sampling location is fixed with respect to the inlet; thermal expansion of the oven tube only takes place at the outlet which is not mechanically connected to the sampling system resulting on a temperature independent length of the reaction segment. At this position the actual gas temperature is close to its plateau value; see Fig. 2 in [30]. All reactions are immediately quenched due to the formation of a molecular beam, when gases are expanded into high vacuum (2 differential pumping stages; 10^{-4} and 10^{-6} mbar). The molecular beam is guided to the ion source of an electron impact (EI) time-of-flight (TOF) mass spectrometer (Kaesdorf, mass resolution R = 3000) and species are detected by their exact mass. The ionization energy was set to 10.5 eV (actual value) in order to minimize fragmentation inside the ion source. The system's performance allows for the determination of the elemental composition (C/H/O) of stable and radical species present in the combustion process. The low electron energy, however, does not allow for precise determination of the major species (H_2O, CO_2, CO, H_2, O_2, and fuel). In addition to the TOF detection, a residual gas analyzer (RGA), i.e. a quadrupole mass spectrometer (Hiden, HAL/3F 301), is additionally placed in the ionization chamber to monitor these six species with a higher electron energy (70 eV) simultaneously to the TOF measurements.

Quantitative data evaluation follows the well-established procedures of flame measurements described in [31,32] and for reactor measurements [33,34], so only an overview is given here.

The integrated and corrected ion signal S of a specific species i is linked to its mole fraction x by comparison with a respective signal of a reference species (Ar). Note that, Ar can be measured even at nominal 10.5 eV due to the broad energy distribution of the ionizing electrons and the high Ar concentration. Signals have been corrected for background and, when necessary, for contributions of ^{13}C isotopes. Additional corrections for ion fragmentation have also been applied when necessary, especially for the RGA data.

Major species (product, reactant) are calibrated by direct cold gas measurements except for H_2O, where an internal calibration strategy relying on the H- and O-balances (depending on the stoichiometry) has been used for calibration. All hydrocarbon intermediates are also calibrated by direct cold gas measurements of either commercial calibration mixtures or binary hydrocarbon/Ar flows, metered by the available Coriolis mass flow controllers. Formaldehyde has been produced and calibrated by quantitative deoligomerization of trioxan $(CH_2O)_3$. For all other oxygenated species the calibration is performed using the "RICS" method (relative ionization cross section) [30,35], which is based on the measurement of electron ionization efficiency curves of chemically similar reference species.

Statistical and relative uncertainties for MBMS signals are typically below 10% [24,30] as the standard deviation for poor signal-to-noise ratios is around 10%. Therefore, a relative comparison of each species offers high precision. Absolute uncertainty is highly dependent on the individual calibration of the distinct species, ranging from 15-20% for direct (cold gas) calibrated and major species, up to uncertainties in the order of factors 2-4 when ionization cross sections for non-direct calibrated intermediates species (RICS) have to be estimated. In total, C and O atom balances deviate from the inlet composition by less than 5% for the measured product composition (RGA data).

For the comparison of the experimental data with the kinetic model, centerline temperature profiles are used as input for the plug flow reactor model (see Sec. 4). These profiles are obtained by a scaling approach that is used to correct an experimental (thermocouple) temperature profile for the actual gas temperature with respect to a given oven temperature T_{Oven}. This scaling approach is discussed in detail in [30] and accounts for effects like thermal inertia of the system or absolute offset. Note that due to the high dilution temperature profiles are independent from the investigated fuel and the applied input temperature profiles can be found as electronic supplement of ref. [36]. The plug flow approximation is based on the measured residence time distribution of the system, which determines a Bodenstein number of Bo~100, often considered as a lower limit for plug flow assumption. Additionally, the previous successful simulations using the plug flow approximation for well-known systems like CH_4 and C_2H_6 has given us additional confidence in proper theoretical treatment of the reactor system [30].

3. Reaction Mechanism of Ethylene Glycol

3.1 Previous mechanism (*Hafner-model*)

The reaction kinetic model of ethylene glycol originates from the work of S. Hafner [5]. This reaction mechanism was developed based on the reactions and rate coefficients of ethanol and similar systems. Due to lack of experiments to characterize combustion properties of EG directly, the reaction model validation was restricted to the sub-system of acetaldehyde, and ethanol at the time. They were considered to be the major intermediates formed during EG decomposition pathways. The details on the reaction model development and validation can be found in Hafner et al. [5,6]. This reaction mechanism will be hereafter referred to as the *Hafner-model*.

3.2 Modifications to the Hafner-model (*Modified-Hafner-model*)

Though the *Hafner-model* was complete, it poses difficulty to many numerical solvers leading to no solution in combustion simulations. In order to render the model more numeric-friendly, we initiated the analysis of the system. It was found that about 40 reactions were responsible for the numerical instability. The reason was large difference in the reverse reaction rates of few species over the temperature range of 300 to 2000 K which were calculated from the forward rate and equilibrium constant in the thermo-database provided together with the *Hafner-model*. These rates were differing as much as 30 orders from 300 – 2000 K temperature range. The thermo-data of species such as $HOCH_2CHOH$, $HOCH_2CH_2O$, $HOCH_2CO$, HOCHCHO, HOCHCO, $HOCH_2CHO$, and CHOCHO were not available at the time Hafner had developed the model and were estimated or taken roughly from the similar species. Therefore, the entire thermo-database was revised [37]. The C_1-C_4 reaction model in the *Hafner-model* was updated to the latest data available [38], improved for a better prediction of acetylene [38,39] important for rich reaction chemistry, also important for the gasification. This model is further improved based on the experiments presented in this work and the resulting model predictions are shown in the Result section.

3.3 Reduced skeletal model for CFD use

The detailed reaction model of EG including C_1-C_4 chemistry contains 78 species and 574 forward reactions. For the mechanism reduction, the reaction mechanism reduction module of chemical workbench [40] was used with Directed Relation Graph (DRG) method [41]. This reaction mechanism is reduced with a target to keep prediction of ignition delay time and the

speciation data of EG closer to the detailed mechanism. The final reduced skeletal model contains 43 species and 270 reactions. The reduced model performs within maximum of 20% uncertainty compared to the detailed model. Additional information on validation target and performance of the reduce model is provided in the Supplemental Material.

4. Combustion modeling

Reaction kinetics of the zero-dimensional (0-D) homogeneous closed reactor model for predicting ignition delay times and flow reactor species data presented here are calculated using Chemical WorkBench (CWB) [40]. Ignition delay times are calculated based on a 0-D homogeneous constant volume reactor model with the initial mixture composition, the initial temperature behind the reflected shock wave, and the pressure profile as input. The ignition delay times are determined from the maximum of CH profiles.

For the flow reactor calculations, the spatial reactor gas temperature profiles for a specific oven temperature [30] is used as an input parameter in addition to initial fuel composition, flow rates, and pressure. There, the correct actual residence times are considered. The calculations are performed at oven temperatures from 750 to 1200 K with intervals of 10 K and the species mole fraction exiting the reactor i.e. at 147 cm are plotted for each initial temperature thereby providing the spectrum of the mole fractions against the oven temperature. All the flow reactor calculations are performed with CWB.

5. Results

Due to the lack of any experimental data, understanding on the evolution of EG model during oxidation was based on analogies [5,6]. The experiments performed in the present work have

been most helpful to overcome this difficulty. The quantitative species profiles obtained in the flow reactor provided important hints on the possible fuel decomposition pathways to the final product spectrum which was impossible to visualize without experiments.

The final mechanism presented here is developed based on the prediction of species in the flow reactor and validated against the ignition delay times. The reactions and species added or modified in the model are explained in detail in result section.

5.1 Ignition delay times

The measurements of ignition delay times in the shock-tube are performed using stoichiometric EG-air mixtures where the synthetic air composition is 80% N_2 and 20% O_2. For the simulations, in order to account for the pressure rise in the experiment, a pressure profile is used as input. The results of the ignition delay times calculations compared to the measurements in the temperature range of 800 to 1500 K and at a pressure of 16 bar are shown in Figure 2. The detailed reaction model fully reproduces the measured ignition delay times in the entire temperature range. The recovery rate of EG from the shock-tube is determined to be 77(±12)% (see section 2.1). Products of the fuel degradation within the EG/O_2/N_2 – mixture preparation period could not be determined (see section 2.1). Thus the actual mixture stoichiometry with respect to EG will be slightly lower than the nominal stoichiometry (Φ = 1.0). Therefore in the calculations, the initial mixture composition is taken and the sensitivity of the fuel stoichiometry is presented instead to see the effect of the recovery rate. The sensitivity of the EG ignition delay times on fuel stoichiometry is evaluated at the nominal experimental mixture stoichiometry of Φ = 1.0 and compared to ignition delay times for fuel-lean (Φ = 0.5) and fuel-rich mixture (Φ = 2.0) for the sake of completeness. As seen in Figure 2, the influence of the fuel stoichiometry on the EG

ignition delay times is small. In addition, the ignition delay times obtained from the reduced mechanism containing 43 species and 270 reactions are also seen to preserve the ignition delay times of detailed mechanism. Details on the reduced model are provided in the Supplemental Material.

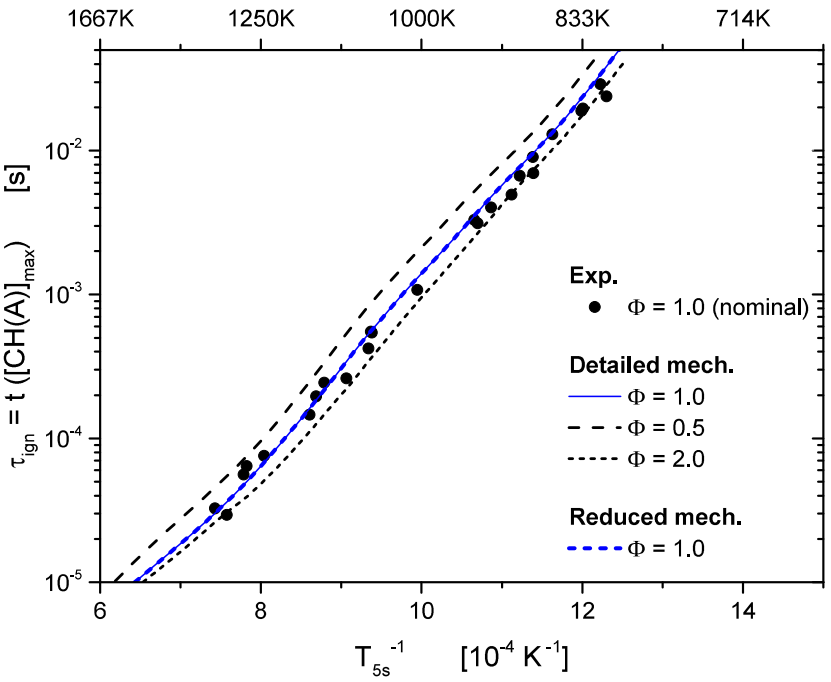

Figure 2: EG – comparison of measured (symbols) and computed (lines) ignition delay times for stoichiometric fuel/ synthetic air mixtures at Φ = 1.0, diluted in 1:2 nitrogen (*p* = 16 bar). To show sensitivity of the fuel stoichiometry on ignition delay times of EG, calculations for Φ = 0.5 and 2.0 are added. The predictions of reduced model are also plotted.

5.2 Species profiles in flow reactor

Species profiles of various intermediates, fuel, oxidizer, and products were obtained at atmospheric conditions in the flow reactor for two fuel stoichiometries, Φ = 1.0 and 2.0. These

profiles are numerically simulated and compared with the experiments. Both are presented in Figures 3 to 10 as a function of the respective oven temperature at given stoichiometry and are classified by their appearance in the fuel consumption path or by similarity in their classes. Figures 3 and 4 show the profiles of EG, O_2, products such as CO_2, H_2O, CO, and H_2 whereas several small alkane or alkene intermediates are presented in Figure 5 and 6. The oxygenated species are the direct decomposition product of either fuel or first fuel radicals (Figure 7 and 8) whereas di-oxygenates species are formed during the oxidation process from the H-abstraction of the fuel (Figure 9 and 10).

5.2.1 Major species

From the Figures 3 and 4 one can see that the measured fuel conversion starts at about 725 K (for $\Phi = 1.0$) and at 675 K (for $\Phi = 2.0$). The initial consumption of the fuel EG is well reproduced by the model up to 850 K and at higher temperature the conversion is faster in the model compared to the experiments. A correct estimation of EG decomposition by the model is impossible at this stage due to unavailability of branching ratios of EG decomposition between H-abstraction and decomposition rates. The conversion of oxygen is slow at low temperatures and is entirely completed at high temperatures.

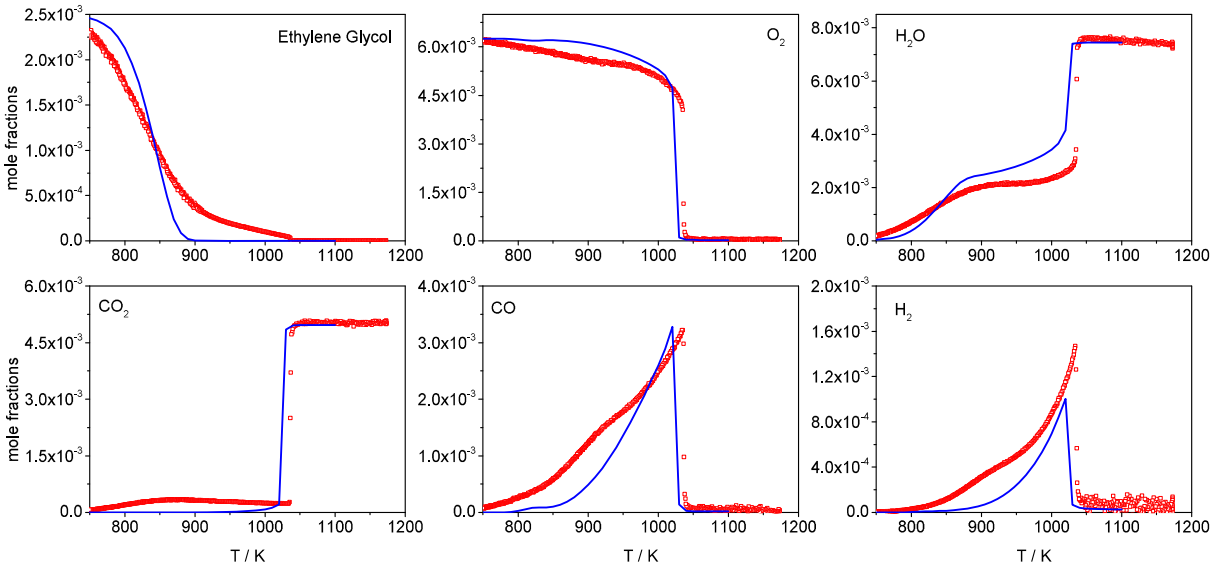

Figure 3: Mole fraction profiles of fuel, O_2, and major products CO, CO_2, and H_2O and the major species H_2 for Φ = 1.0 as a function of the respective oven temperatures (T). Symbols represent experimental data and lines modeling results. No scaling factor or T-shift is applied.

In the flow reactor, the subsequent formation of products H_2, H_2O, CO, and CO_2 is increasing as expected at high temperatures. Few species formations, as predicted by the model, are influenced by the direct fuel or by the first fuel radicals (C_2H_4O, CH_3CO, $HOCH_2CHOH$, and $HOCH_2CHO$) chemistry. In the model, H_2 formations at different temperatures are from reactions EG → H_2 + $HOCH_2CHO$ (750 – 810 K), CH_3CHO + H → H_2 + CH_2CHO/CH_3CO (820 – 950 K), CH_3HCO + H → H_2 + CH_2HCO/CH_3CO (960 – 1010 K) and for higher temperatures (1010 – 1030 K) by CH_2O + H → H_2 + HCO reaction. Only beyond 1040 K, the hydrogen chemistry plays a prominent role. Thus, the H_2 formation is ruled by either fuel decomposition or H-abstraction of the fuel products (CH_3CHO, CH_2O). Similarly, the formation of CO is dominated mainly by the decomposition of CH_3CO which is a major product of acetaldehyde. Only beyond 990 K, the HCO + O_2 reaction leads to CO formation. Thus the EG chemistry indirectly influence the CO

formation. In measured CO, CO_2, and H_2 profiles, one sees a faint first region of plateaus between 800 and 950 K. However, the model is unable to reproduce the first plateau in all this three profiles. We assume this to be related to unavailability of reaction rates to facilitate correct temperature dependence of EG consumption.

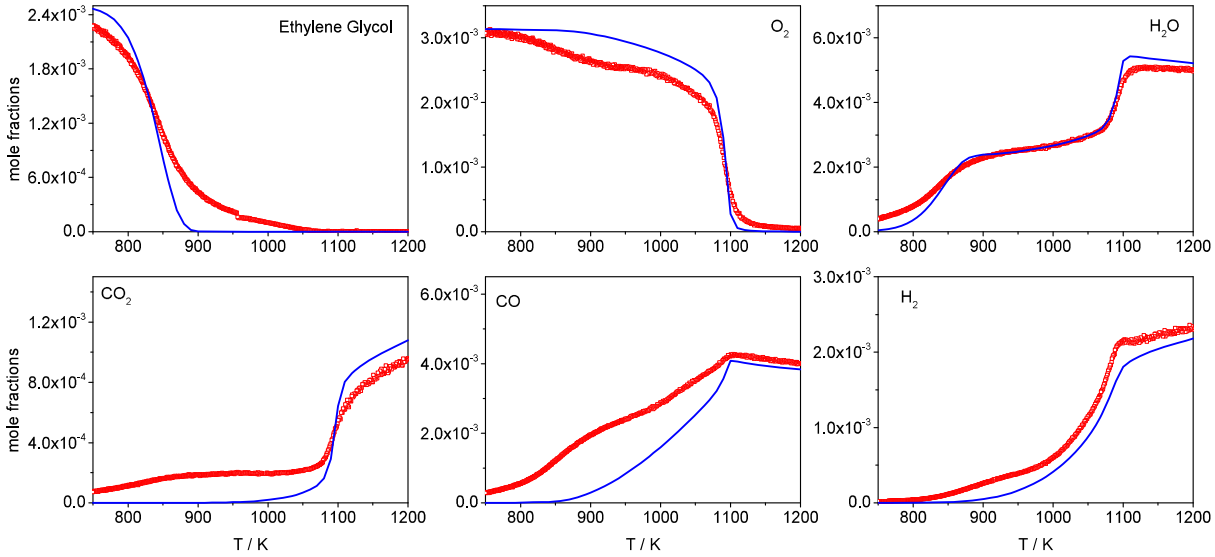

Figure 4: Mole fraction profiles of fuel, O_2, and major products CO, CO_2, and H_2O and the major species H_2 for Φ = 2.0 as a function of the respective oven temperatures (T). Symbols represent experimental data and lines modeling results. No scaling factor or T-shift is applied.

Figures 3 and 4 show measured profiles of H_2O with two different regions of plateaus; here the first plateau is prominent. The model analysis shows that the first smaller plateau lies in the region of 700 – 1050 K where predominant source is either the fuel decomposition reaction i.e. EG → CH_3HCO + H_2O or the abstraction reaction CH_3HCO + OH → CH_3CO + H_2O. Above 1000 K when the fuel is almost decomposed, bimolecular reaction: CH_2O + OH → HCO + H_2O and later reactions from hydrogen sub-system forms H_2O. Compared to this, the EG reaction

system has no direct influence on CO_2 formation. At all temperatures, the CO_2 is formed by oxidation of CO.

5.2.2 C_1-C_4 Hydrocarbon species

The intermediate hydrocarbons measured are CH_4, C_2H_2, C_2H_4, and C_2H_6 (Figure 5 and 6) which except acetylene, shows maximum concentration at intermediate temperatures and complete consumption beyond 1100 K. Compared to them, acetylene is formed at higher temperatures only. The model prediction shows only CH_4 is directly influenced by the EG chemistry through the H-abstraction reactions of CH_3HCO by CH_3 radicals (800 to 1000 K). Both modeled C_2H_4 and C_2H_6 are formed through the paths typical to hydrocarbon oxidation and are in excellent agreement with the measurements. Acetylene, an important intermediate in the soot formation is under predicted by the simulations at rich condition (Figure 6) compared to the measurements. The measured C_2H_2 profile exhibits rapid increase above 1020 K. In our previous work on rich methane oxidation [34], the acetylene showed a similar rapid rise in concentration followed by a plateau at higher temperatures beyond 1350 K. It is well known that at flame conditions, acetylene is usually formed from the C_2H_3 radical via $C_2H_3 + M \rightarrow C_2H_2 + H + M$ which is the final step in the consecutive dehydrogenation chain starting from the methyl radical to formation of ethane due to methyl radical recombination [42-44]. Although the simulated C_2H_2 profile is in agreement with the measured ones till 1290 K, it further drops followed by a second rise (lower by factor of 3) not seen in the measurement. We found that in the model the acetylene consumption channel ($C_2H_3 + M \rightarrow C_2H_2 + H + M$) is more dominant than formation, which in fact should be reversed. By deliberately suppressing this reaction (only forward route implemented), the acetylene formation follows the known formation route through

$CH_3 \rightarrow C_2H_6 \rightarrow C_2H_5 \rightarrow C_2H_4 \rightarrow C_2H_3 \rightarrow C_2H_2$ and consumption mainly by HCCO. In addition, the reactions of CH_2HCO are also important to acetylene formation. In general, revising the $C_2H_3 + M \rightarrow C_2H_2 + H + M$ reverse rate and the rates of three reactions $C_2H_3 + O \rightarrow CH_2O + HCO/CH_2HCO + O/C_2H_2 + HO_2$, lead to proper consumption of C_2H_3 to C_2H_2 (seen in Figure 6 as dotted lines). Though this is not enough, as some discrepancies still remains related to larger C_3-C_4 hydrocarbons.

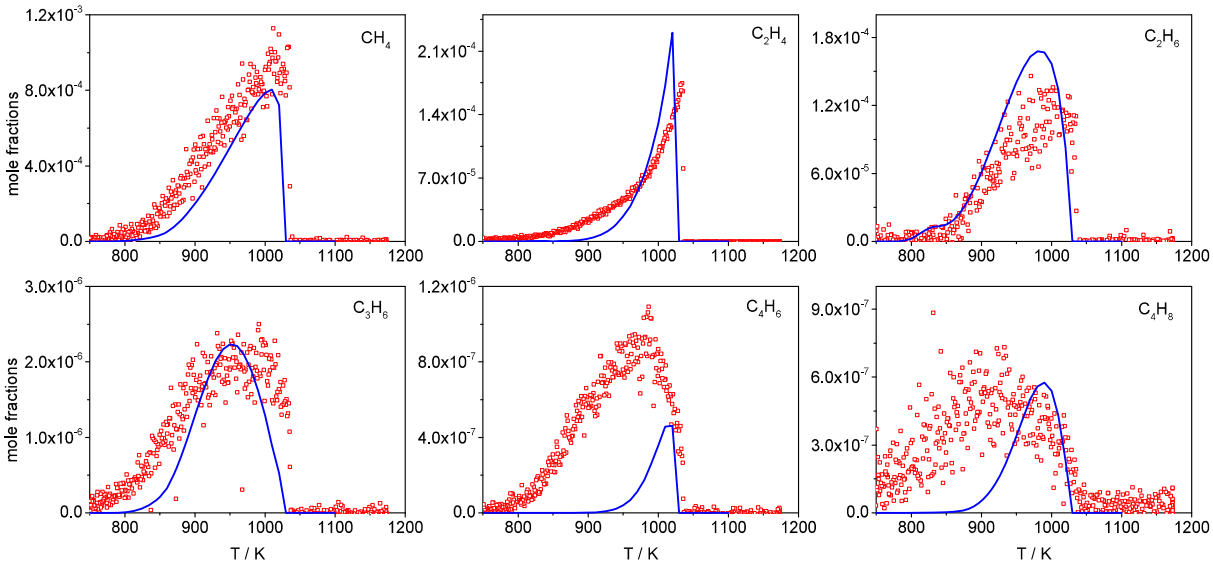

Figure 5: Mole fraction profiles of C_0-C_4 hydrocarbon intermediates as a function of the respective oven temperatures (T) for $\Phi = 1.0$. Symbols represent experimental data and lines modeling results. No scaling factor or T-shift is applied.

Among larger hydrocarbons, C_3H_6, C_4H_6, and C_4H_8 are measured in the flow reactor (Figure 5 and 6). The major path to C_3H_6 formation is the reaction $CH_3HCO + CH_3 \rightarrow C_3H_6 + OH$ and is very well reproduced by the model. The formation of C_4H_6 occurs through C_4H_7 radical whereas C_4H_8 through AC_3H_5 and is not seen to be reproduced by the simulations beyond 1000 K. In general rich C_3-C_4 hydrocarbon base chemistry needs revision.

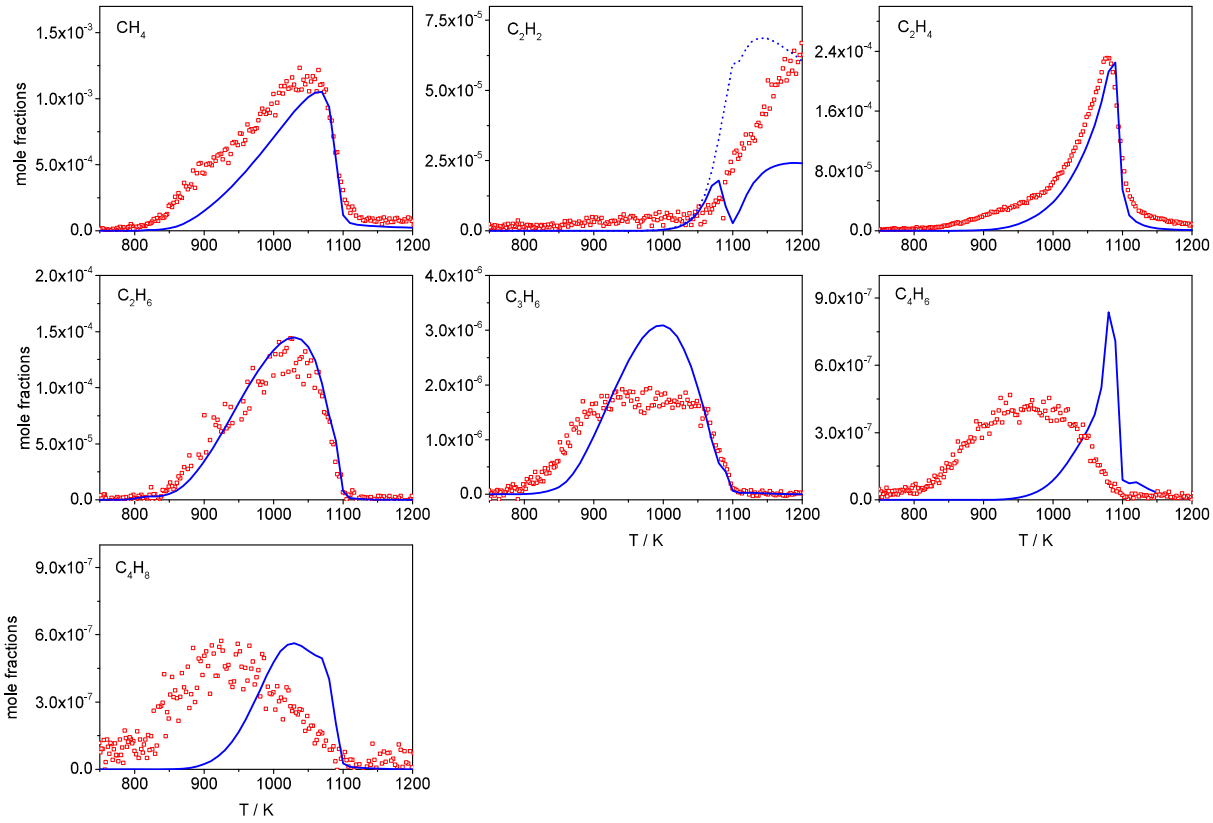

Figure 6: Mole fraction profiles of C_0-C_4 hydrocarbon intermediates as a function of the respective oven temperatures (T) for Φ = 2.0. Symbols represent experimental data and lines modeling results (dotted lines modifications related to C_2H_2 reactions described in text). No scaling factor or T-shift is applied.

5.2.3 Oxygenated species

Among the five oxygenated species measured (Figure 7, 8), the profiles of CH_4O, C_2H_2O, and C_2H_4O are seen to be formed immediately as the fuel conversion starts and therefore can be interpreted as a direct or indirect product of EG. This is also seen in the model where the major formation reactions are EG → CH_3OH + CH_2O, $HOCH_2CHO$ → CH_2CO + H_2O, and EG → CH_3HCO + H_2O, respectively. Based on observations from the experiments, few possible paths

were added to the model. The formation of CH_2CO through decomposition of 2-hydroxyethanal ($HOCH_2CHO \rightarrow CH_2CO + H_2O$), which is an intermediate of fuel H-abstraction channel, is seen as a possible route and is inserted in the model. The formation of CH_2CO through the regular H-abstraction of CH_2HCO channel ($CH_2CO + R \rightarrow CH_2CO + RH$) is not possible even when changing the reaction rates by 2 to 3 orders of magnitude.

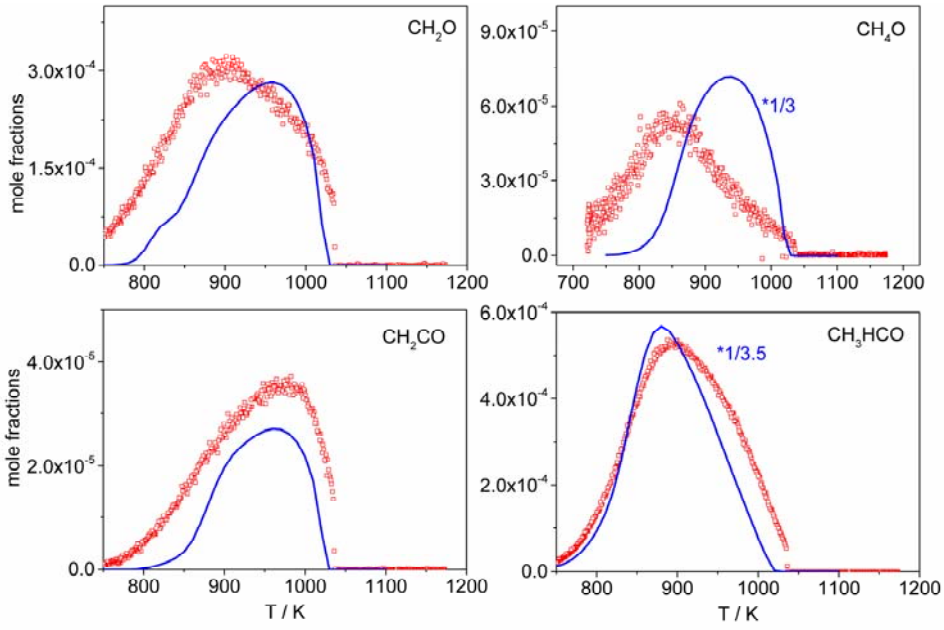

Figure 7: Mole fraction profiles of oxygenated intermediates as a function of the respective oven temperatures (T) for $\Phi = 1.0$. Symbols represent experimental data and lines modeling results. To facilitate comparison of the respective trends, a scaling factor (model data scaled roughly to maximum experimental value) is indicated when applied, no T-shift applied.

The predicted concentrations of CH_3HCO and CH_4O species are about 3 times higher than the measurements. This could be due to measurement uncertainties but also model uncertainties related to the absence of enol chemistry. Nevertheless, this can only be confirmed through

identification of C_2H_4O isomers experimentally in the future work. The formation of modeled CH_2O is from the known reaction of $CH_3O + M \rightarrow CH_2O + H + M$.

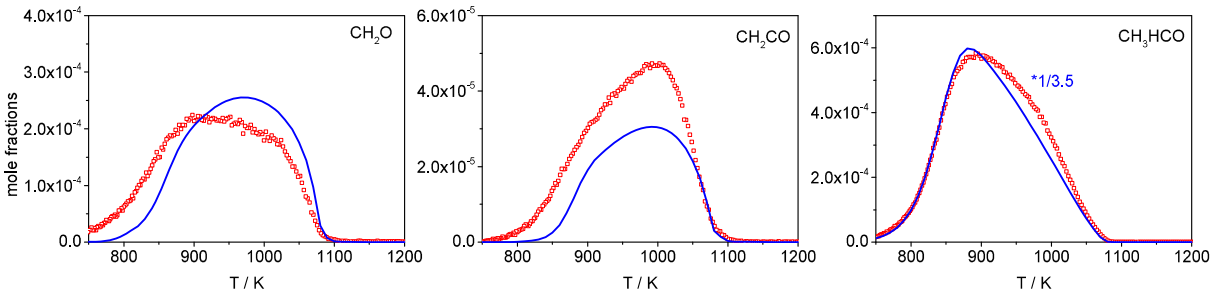

Figure 8: Mole fraction profiles of oxygenated intermediates as a function of the respective oven temperatures (T) for Φ = 2.0. Symbols represent experimental data and lines modeling results. To facilitate comparison of the respective trends, a scaling factor (model data scaled roughly to maximum experimental value) indicated when applied, no T-shift applied.

5.2.4 Di-Oxygenated species

The 2-hydroxyethanal ($HOCH_2CHO$) and ethanedial (glyoxal, CHOCHO) are the two di-oxygenated species that are measured (Figure 9 and 10). Both these species are formed at the lowest measured temperatures and are completely consumed below 1050 K temperatures. Both these species are predicted by the model. Based on the available literature data, Faßheber et al. [45] assembled a reaction mechanism of ethanedial. We replaced the reaction rates of the decomposition and the H-abstraction reactions of ethanedial from their study in our mechanism. Their rates are estimated in the intermediate to high temperature range which is also appropriate for the present study. The entire EG mechanism is insensitive to this sub-part which is apparent as CHOCHO is just an end product of H-abstraction and oxidation reactions starting with the fuel molecule. The only reactions responsible for the formation of 2-hydroxyethanal and ethanedial are the H-abstraction reactions $HOCH_2CHOH + O_2 \rightarrow HOCH_2CHO + HO_2$ and

HOCHCHO + O_2 → CHOCHO + HO_2, respectively. Here, $HOCH_2CHOH$ is the secondary radical formed by H-abstraction of the fuel EG whereas the HOCHCHO radical is a subsequent product of 2-hydroxyethanal. The maximum concentration of $HOCH_2CHO$ is about one order of magnitude higher in the model prediction whereas the ethanedial peak concentration is 3-5 times lower than the measurements. These differences could be due to model uncertainties related to reaction rates of the EG system as well as due to experimental uncertainty, since no ionization cross sections are known. It should be also mentioned at this point that even though the soft ionization conditions are chosen to avoid fragmentation in the ion source of the spectrometer, oxygenates are known to fragment easily which could not be accounted for these species. Considering these facts the uncertainty for di-oxygenated species may be as high as a factor of 4 in the experiment, and thus the simulations may still be in reasonable agreement.

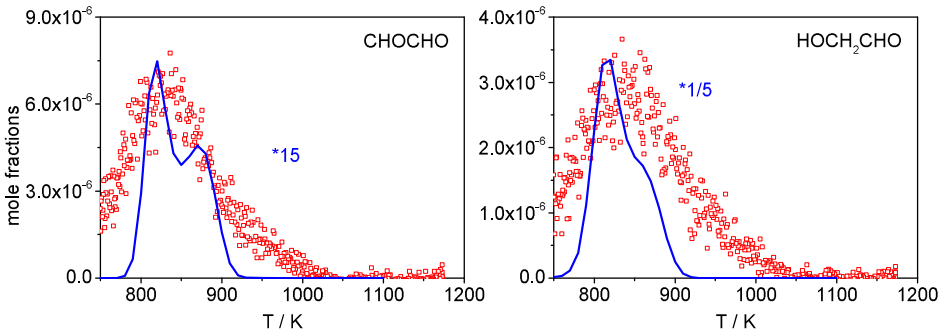

Figure 9: Mole fraction profiles of di-oxygenated intermediates as a function of the respective oven temperatures (T) for Φ = 1.0. Symbols represent experimental data and lines modeling results. To facilitate comparison of the respective trends, a scaling factor (model data scaled roughly to maximum experimental value) indicated when applied, no T-shift applied.

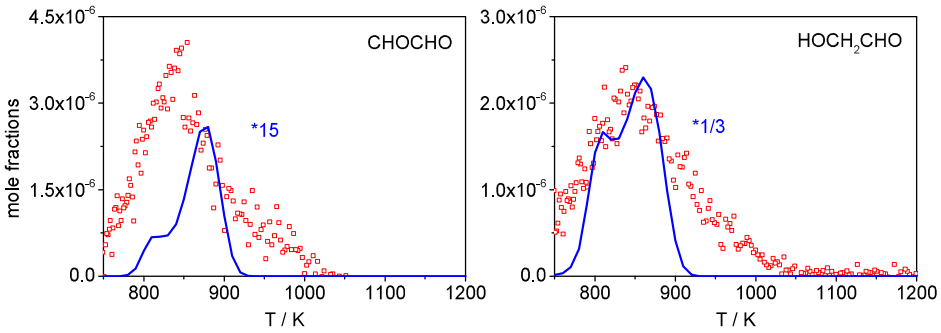

Figure 10: Mole fraction profiles of di-oxygenated intermediates as a function of the respective oven temperatures (T) for Φ = 2.0. Symbols represent experimental data and lines modeling results. To facilitate comparison of the respective trends, a scaling factor (model data scaled roughly to maximum experimental value) indicated when applied, no T-shift applied.

Concluding the flow reactor study in general, good agreement is seen between the measured and the modeled mole fractions of most species studied in this work. This conclusion can also be generalized for rich conditions as no distinct difference is seen to stoichiometric mixtures. Figure 11 shows direct comparison of profiles at stoichiometric and fuel-rich condition. Since the variation in fuel stoichiometry is done by changing the oxygen concentration, the fuel profiles are similar. As expected, at fuel-rich conditions the hydrocarbon intermediates reach higher concentration whereas at oxygen-rich conditions, the concentration of oxygenates are higher. The main combustion products show similar trends in the profile shape. Although there is no significant variation in the intermediate pool, two profiles, namely CO and H_2 show a strikingly similar behavior at rich condition i.e. both are not consumed at higher temperatures. In the rich case, O_2 conversion is slower than in the stoichiometric case. So, an increase in CO and H_2 mole fractions up to 1100 K (temperature when O_2 is completed converted) is expected and is similar to the stoichiometric case where complete conversion of O_2 takes place at ~1025 K. However at

higher temperatures when the O_2 is completely converted, unlike at Φ =1.0 where rapid depletion is seen, the consumption of H_2 and CO is much slower in the rich case. The H_2 mole fraction even keeps increasing unlike in the stoichiometric case where it is completely consumed. The concentration levels of H_2 and CO are due to the radical pool sustained by the remaining CH_4, C_2H_4, and C_2H_2. This differs from the stoichiometric case where all intermediates are completely consumed.

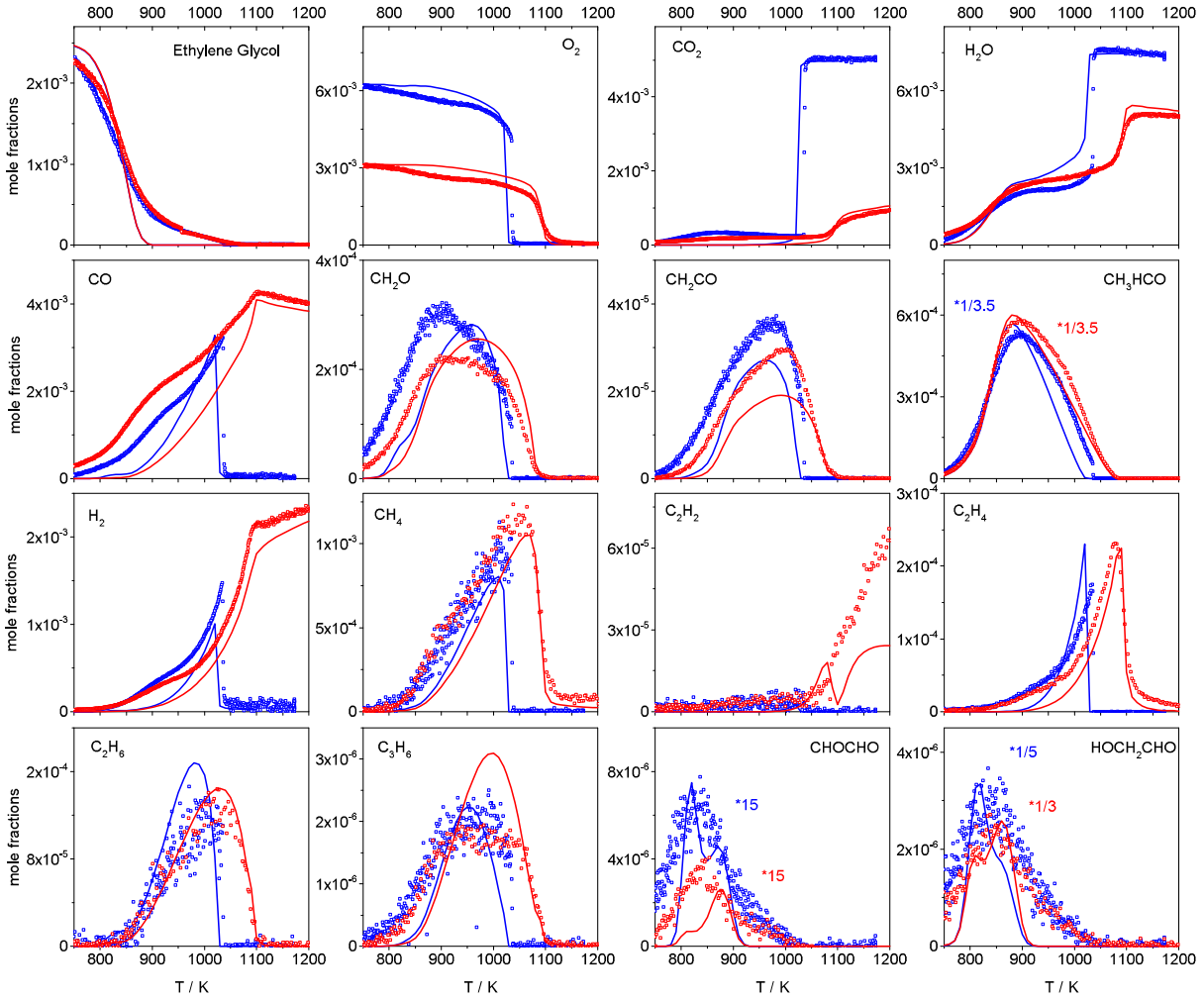

Figure 11: Direct comparison of fuel, oxidizer, products, major species, and intermediates for both fuel stoichiometries measured. Φ = 1.0 (blue), Φ = 2.0 (red).

5.3 Fuel consumption paths

Due to lack of accurate reaction rates of EG reactions, the focus of this study is to understand the fuel consumption of the EG with the help of species measured in a flow reactor. Figure 12 presents reaction path analysis at an oven temperature when the fuel conversion is about 50%.

The EG fuel consumption starts mainly with the decomposition channel forming C_2H_4O and H_2O ($EG \rightarrow C_2H_4O + H_2O$). The formation of first fuel radical by H-abstraction reaction is a second major channel of the fuel conversion ($EG + R \rightarrow HOCH_2CHOH + RH$, where R = H, O, OH, HO_2, O_2, HCO, HCCO). The secondary fuel radical $HOCH_2CHOH$ in a reaction with oxygen forms hydroxyethanal ($HOCH_2CHOH + O_2 \rightarrow HOCH_2CHO + HO_2$) which is the source of ethanedial; both species are measured in the experiments. In addition, in a minor channel, fuel converts via C-C bond breaking to methanol ($EG \rightarrow CH_3OH + CH_2O$) and hydroxyl-methyl radicals ($EG \rightarrow 2CH_2OH$). The acetaldehyde, as a C_2H_4O isomer considered here, converts to the acetyl radical by H-abstraction ($CH_3CHO + R \rightarrow CH_3CO + RH$) which decomposes to give the methyl radical and CO. Thus, H_2O, CO, and CH_4 are seen to be formed immediately when the fuel decomposition has started. The 2-hydroxyethanal is the source of ketene and ethanedial. The C_2-C_3 hydrocarbons formation through methyl radical recombination followed by the H-abstraction reaction is well known. Figure 12 indicates the species measured in the flow reactor by blue boxes. A wide range of the product spectrum of EG decomposition is measured and for most of these species the simulations are in excellent agreement with the measured mole fractions. Thus, the model supplies a basic understanding of EG decomposition chemistry supported by the measurements.

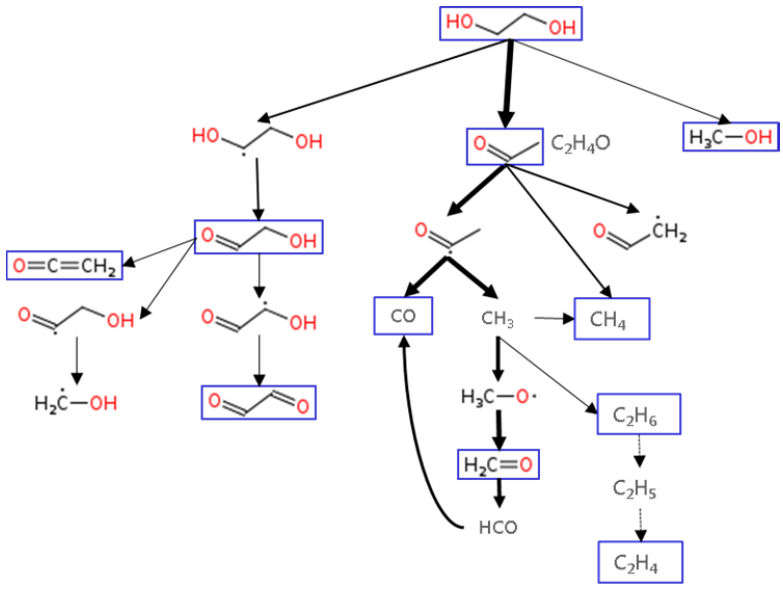

Figure 12: Reaction path analysis for the conditions in the flow reactor at an oven temperature of 840 K (50% fuel conversion). The fuel decomposition paths are very similar for fuel stoichiometries $\Phi = 1.0$ and $\Phi = 2.0$. The species marked with blue boxes are measured in the flow reactor.

6. Discussion

There are certain unique features of EG combustion that are observed in the flow reactor study. The original *Hafner-model* and *Modified-Hafner-model* considered H-abstraction of fuel to the first fuel radicals (EG + R → $HOCH_2CHOH$ (or $HOCH_2CH_2O$) + RH) as dominant fuel consumption channel. When the flow reactor conditions were simulated with these models, no formation of CH_3OH, CH_2CO, CH_3CHO, H_2, CH_4, C_2H_2, C_2H_4, C_2H_6, C_3H_6, C_4H_6, and C_4H_8 was seen at any oven temperature. However, the experiments clearly proof the formation of all of these species. Additionally, in experiments, some of these species such as CH_3OH and CH_3CHO formation were seen almost immediately as the fuel conversion has started. Four fuel decomposition reactions EG → $2CH_2OH$, EG → CH_2CH_2OH + OH, EG → CH_3CHO + H_2O,

and EG → $HOCH_2CHO$ + H_2 were part of original mechanisms, but were not dominant compared to the H-abstraction routes. The measured profiles pointed that if the fuel decomposition is dominant fuel conversion channel, it will explain the formation of above non-existent species in the earlier models. This leads to an inference that the fuel decomposition channel is at least as important as the H-abstraction channel. This was further strengthened by the fact that the H_2O profile has two distinct plateaus, the first one seen in the temperature region of complete fuel conversion which is directly related to H_2O formation via EG → C_2H_4O + H_2O reaction (Figure 3 and 4). The additional OH in the EG molecule compared to ethanol has an extra effect on easy H_2O elimination.

Though the fuel decomposition reactions were present in the earlier models, their rates were not dominant compared to the H-abstraction rates. We incorporated the EG decomposition reaction rates (for reactions EG → C_2H_4O + H_2O, EG → $2CH_2OH$) predicted by Ye et al. [15] but the H-abstraction rates were still dominant compared to the decomposition rates and would require abstraction rate of at least one reaction (EG + R → $HOCH_2CHOH$ + RH) to be 4 orders of magnitude larger to see decomposition dominant. Based on these observations, the activation energy and temperature exponent of the reaction rates of above decomposition reactions of EG are calculated using the open-source reaction model generation software RMG [46] for the reaction EG → C_2H_4O + H_2O and the A-factor was modified depending on the product concentration found in the experiment.

An Arrhenius diagram showing comparison of EG → C_2H_4O + H_2O reaction rates by Ye et al. [15], the RMG-rate, and the modified-RMG-rate are shown in Figure 13. For EG → C_2H_4O + H_2O reaction we modified RMG-rate by factor of ~0.5. Comparison of these three rates at atmospheric condition shows large differences between RMG- and Ye-rates. For 700 – 1000 K,

the differences are as large as order of 9. At lower temperatures (<700 K) the differences are even larger. The Ye-rate at 10 atmospheres is comparable to RMG rates (factor of 3 at 700 K, one order at 1000 K).

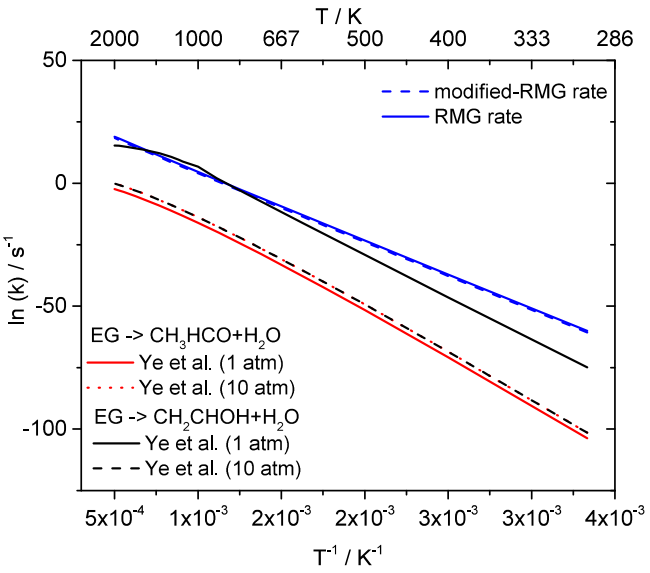

Figure 13: Reaction rate coefficients comparison of EG → C_2H_4O + H_2O reaction.

In comparison, H-abstraction rates of EG are not available in literature except at atmospheric chemistry condition [47,48] and these room temperature reaction rates are insufficient for combustion relevant conditions. Therefore, for the present study we estimated them by the collision theory. The purpose was to understand the reaction routes of EG based on the experiments we performed and provide recommendation for the improvement.

Based on the product spectrum found in the flow reactor we estimate following reactions to be dominant decomposition routes which are also supported by the theoretical rate estimations of Ye et al. [15]:

EG → C_2H_4O+ H_2O

EG → CH_3OH + CH_2O

EG → 2CH_2OH

$EG \rightarrow HOCH_2CHO + H_2$

The direct decomposition of the fuel EG leads to the $C_2H_4O + H_2O$ reaction. Both acetaldehyde and ethenol can be identified as isomers of C_2H_4O that play an important role as direct decomposition products. Since the present experiment cannot distinguish among these isomers, it therefore remains unclear at present.

There are two important aspects that need attention in the future with respect to EG decomposition:

- Experimental identification of C_2H_4O isomers formed from EG. Does the product distribution of both these isomers have an effect on the intermediate radical pool? Stability of CH_2CHOH, over a wide temperature and pressure range is theoretically possible, given the reaction rates of EG decomposition available in the literature as *f*(T,p). But in absence of EG H-abstraction rates this information is not sufficient and as the branching to both of these channels is unclear.
- Reaction rate of EG abstraction reactions by H-atom at combustion temperatures would be helpful in modeling EG kinetics. So far, only room temperature rate are available. Such investigation will help to get the correct branching ratio of the H-abstraction to the decomposition channel of EG fuel consumption which is important for the radical pool generated further on. We are currently doing calculations of the H-abstraction reaction rates of EG and its decomposition processes based on the quantum chemical calculations.

7. Conclusions

Ethylene glycol (EG) is investigated in this work as a surrogate fuel for pyrolysis oil important in numerical studies of gasification processes. In absence of any kinetic information on EG, a

detailed reaction mechanism is optimized based on the information provided by the first ever experiments performed in the EG system. The two types of experiments undertaken are, ignition delay times measurements in a shock-tube at 16 bar over a temperature range of 800 – 1500 K at stoichiometric condition and systematic speciation data obtained by the DLR high temperature flow reactor setup with coupled MBMS detection for stoichiometric (Φ = 1.0) and fuel rich (Φ = 2.0) EG conditions. These new experiments supply an important database on the ignition delay times as well as quantitative species profiles of various major products and intermediates. They provide indirect inference on how the EG oxidation can be better explained at given conditions. The detailed reaction model is first time tested against the experimental data of EG and is found to reproduce the measurements with excellent agreement. In addition, a skeletal reaction scheme is obtained from the detailed reaction model reduced to about 50% in number of species which is useful for CFD simulations of gasification processes. Additional data on the validation of the reduced skeletal mechanism is available as Supplemental Material.

8. Acknowledgements

C. N. and T. K. thanks Norbert Ackermann and Heiko Dreyer for helping with experiments, EG-analysis and probing. P. O. and M. K. wish to thank the DLR Center of Excellence “Alternative Fuels” for financial support.

9. References

[1] COM(2014) 520 final communication on Energy Efficiency and its contribution to energy security and the 2030 Framework for climate and energy policy, European commission report, Online at: https://ec.europa.eu/energy/en/topics/renewable-energy.

[2] T. Kolb, B. Zimmerlin, SGC Gasification Seminar, Malmö, Sweden, October 15–16 (2014).

[3] T. Kolb, M. Aigner, R. Kneer, M. Mueller, R. Weber, N. Djordjevic, Tackling the challenges in modelling entrained-flow gasification of low-grade feedstock, J. Energ. Inst., 89 (2016) 485-503.

[4] U. Santo, H. Seifert, T. Kolb, L. Krebs, D. Kuhn, H. Wiemer, E. Pantouflas, N. Zarzalis, Conversion of biomass based slurry in an entrained flow gasifier, Chem. Eng. Technol., 30(7) (2007) 967–969.

[5] S. Hafner, Modellentwicklung zur numerischen Simulation eines Flugstromvergasers für Biomasse Ph.D. Thesis, Universität Heidelberg (2010).

[6] S. Hafner, A. Rashidi, G. Baldea, U. Riedel, A detailed chemical kinetic model of high-temperature ethylene glycol gasification, Combust. Theor. Model. 15 (2011) 517–535.

[7] H. Wang, J. Male, Y. Wang, Recent advances in hydrotreating of pyrolysis bio-oil and its oxygen-containing model compounds, ACS Catal. 3 (2013) 1047–1070.

[8] A. Oasmaa, S. Czernik, Fuel oil quality of biomass pyrolysis oils-State of the art for the end users, Energ. Fuels, 13 (4) (1999) 914–921.

[9] American Institute of Chemical Engineers (AIChE), Evaluated Process Design Data, Public Release Documentation, Design Institute for Physical Properties (DIPPR), Project 801 (2006).

[10] M. Kaltschmitt, H. Hartmann und H. Hofbauer, Energie aus Biomasse: Grundlagen, Techniken und Verfahren, (2009) 2nd Edition, Springer, ISBN 978-3-540-85094-6, 686.

[11] F. Yu, S. Deng, P. Chen. Y. Liu, Y. Wan, A. Olson, D. Kittelson, R. Ruan, Physical and chemical properties of bio-oils from microwave pyrolysis of corn stover, Appl Biochem. Biotechnol., 137-140 (1-12) (2007) 957–970.

[12] C. Mullen, A. Boateng, Chemical composition of bio-oils produced by fast pyrolysis of two energy crops, Energ. Fuels, 22 (2008) 2104–2109.

[13] ASTM D7544 – 12, Standard Specification for Pyrolysis Liquid Biofuel, http://www.astm.org/Standards/D7544.htm.

[14] J. Park, R. S. Zhu, and M. C. Lin, Thermal decomposition of ethanol. I. Ab Initio molecular orbital/Rice–Ramsperger–Kassel–Marcus prediction of rate constant and product branching ratios, J. Chem. Phys. 117 (2002) 3224–3230.

[15] L. Ye, L. Zhao, L. Zhang, F. Qi, Theoretical studies on the unimolecular decomposition of ethylene glycol, J. Phys. Chem. A, 116 (2012) 55–63.

[16] T.A. Cool, K. Nakajima, T.A. Mostefaoui, F. Qi, A. McIlroy, P.R. Westmoreland, M.E. Law, L. Poisson, D.S. Peterka, M. Ahmed, Selective detection of isomers with photoionization mass spectrometry for studies of hydrocarbon flame chemistry, J. Chem. Phys., 119 (2003) 8356–8365.

[17] C.A. Taatjes, N. Hansen, A. McIlroy, J.A. Miller, J.P. Senosiain, S.J. Klippenstein, F. Qi, L. Sheng, Y. Zhang, T.A. Cool, J. Wang, P. R. Westmoreland, M.E. Law, T. Kasper, K. Kohse-Hoeinghaus, Enols are common intermediates in hydrocarbon oxidation, Science 308 (2005) 1887–1889.

[18] C.A. Taatjes, N. Hansen, J.A. Miller, T.A. Cool, J. Wang, P. R. Westmoreland, M.E. Law, T. Kasper, K. Kohse-Hoeinghaus, Combustion chemistry of enols: Possible ethenol precursors in flames, J. Phys. Chem. A, 110 (9) (2006) 3254–3260.

[19] G. da Silva, C. Kim, J.W. Bozzelli, Thermodynamic properties (Enthalpy, Bond Energy, Entropy, and Heat Capacity) and internal rotor potentials of vinyl alcohol, methyl vinyl ether, and their corresponding radicals, J. Phys. Chem. A 110 (2006) 7925–7934.

[20] A. Vasiliou, K.M. Piech, X. Zhang, M.R. Nimlos, M. Ahmed, A. Golan, O. Kostko, D.L. Osborn, J.W. Daily, J.F. Stanton, G.B. Ellison, Thermal decomposition of CH3CHO studied by matrix infrared spectroscopy and photoionization mass spectroscopy, J. Chem. Phys. 135 (2011) 014306-1–014306-5.

[21] R. Sivaramakrishnan, J.V. Michael, L.B. Harding, S.J. Klippenstein, Resolving some paradoxes in the thermal decomposition mechanism of acetaldehyde, J. Phys. Chem., A 119 (2015) 7724−7733.

[22] T. Tao, W. Sun, B. Yang , N. Hansen, K. Moshammer, C.K. Law, Investigation of the chemical structures of laminar premixed flames fueled by acetaldehyde, Proc. Combust. Inst., (2016), doi: 10.1016/j.proci.2016.05.030.

[23] R. Sivaramakrishnan, M.C. Su, J.V. Michael, S.J. Klippenstein, L.B. Harding, B. Ruscic, Rate constants for the thermal decomposition of ethanol and its bimolecular reactions with OH and D: Reflected shock tube and theoretical studies, J. Phys. Chem. A, 114 (35) (2010) 9425–9439.

[24] N. Hansen, T. A. Cool, P. R. Westmoreland, K. Kohse-Höinghaus, Recent contributions of flame-sampling molecular-beam mass spectrometry to a fundamental understanding of combustion chemistry, Prog. Energy Combust. Sci. 35 (2009) 168–191, doi: 10.1016/j.pecs.2008.10.001.

[25] B. Yang, C.K. Westbrook, T.A. Cool, N. Hansen, K. Kohse-Hoeinghaus, Fuel-specific influences on the composition of reaction intermediates in premixed flames of three C 5 H 10 O 2 ester isomers, Phys. Chem. Chem. Phys., 13 (2011) 6901–6913.

[26] Y. Li, L. Wei, Z. Tian, B. Yang, J. Wang, T. Zhang, F. Qi, A comprehensive experimental study of low-pressure premixed C3-oxygenated hydrocarbon flames with tunable synchrotron photoionization, Combust. Flame 152 (2008) 336–359.

[27] P. Oßwald, P. Hemberger, T. Bierkandt, E. Akyildiz, M. Köhler, A. Bodi, T. Gerber, T. Kasper, In situ flame chemistry tracing by imaging photoelectron photoion coincidence spectroscopy, Rev. Sci. Instrum. 85 (2) (2014) 025101, doi: 10.1063/1.4861175.

[28] F. Qi, Combustion chemistry probed by synchrotron VUV photoionization mass spectrometry, Proc. Combust. Inst. 34 (2013), 33–63.

[29] J. Herzler, L. Jerig, P. Roth, Shock tube study of the ignition of lean n-heptane/air mixtures at intermediate temperatures and high pressures, Proc.Comb.Inst., 30 (2005) 1147–1153.

[30] P. Oßwald, M. Köhler, An atmospheric pressure high-temperature laminar flow reactor for investigation of combustion and related gas phase reaction systems, Rev. Sci. Instrum. 86 (10) (2015) 105109.

[31] P. Oßwald, H. Güldenberg, K. Kohse-Höinghaus, B. Yang, T. Yuan, F. Qi, Combustion of butanol isomers - A detailed molecular beam mass spectrometry investigation of their flame chemistry, Combust. Flame 158 (1) (2011) 2–15, doi: 10.1016/j.combustflame.2010.06.003.

[32] M. Schenk, L. Leon, K. Moshammer, P. Oßwald, T. Zeuch, L. Seidel, F. Mauss, K. Kohse-Höinghaus, Detailed mass spectrometric and modeling study of isomeric butene flames, Combust. Flame 160 (3) (2013) 487–503, doi: 10.1016/j.combustflame.2012.10.023.

[33] F. Herrmann, P. Oßwald, K. Kohse-Höinghaus, Mass spectrometric investigation of the low-temperature dimethyl ether oxidation in an atmospheric pressure laminar flow reactor, Proc. Combust. Inst. 34 (1) (2013) 771–778, doi: 10.1016/j.proci.2012.06.136.

[34] M. Köhler, P. Oßwald, H.-B. Xu, T. Kathrotia, C. Hasse, U. Riedel, Speciation data for fuel-rich methane oxy-combustion and reforming under prototypical partial oxidation conditions, Chem. Eng. Sci. 139 (2016) 249–260, doi: 10.1016/j.ces.2015.09.033.

[35] J. C. Biordi, Prog. Molecular beam mass spectrometry for studying the fundamental chemistry of flames, Progress Energy Combust. Sci. 3 (3) (1977) 151–173.

[36] P. Oßwald, R. Whitside, J. Schäffer, M. Köhler, An experimental flow reactor study of the combustion kinetics of terpenoid jet fuel compounds: Farnesane, p-menthane and p-cymene , Fuel 187 (2017) 43–50.

[37] E. Goos, A. Burcat, B. Ruscic, New NASA thermodynamic polynomials database with active thermochemical tables updates, Report ANL 05/20 TAE 960 (2011).

[38] T. Kathrotia, Reaction kinetics modeling of OH*, CH*, and C2* chemiluminescence, Ph.D. Thesis, Universität Heidelberg, 2011. Online at: http://archiv.ub.uni-heidelberg.de/volltextserver/12027.

[39] S. Wagner, M. Klein, T. Kathrotia, U. Riedel, T. Kissel, A. Dreizler, V. Ebert, In situ TDLAS measurement of absolute acetylene concentration profiles in a non-premixed laminar counter-flow flame, Appl. Phys. B 107 (2012) 585–589.

[40] Chemical WorkBench® 4.0, Kintech Lab. (2013), http://www.kintechlab.com/products/chemical-workbench/.

[41] A. V. Lebedev, M. V. Okun, V. A. Chorkov, P. M. Tokar. M. Strelkova, Systematic procedure for reduction of kinetic mechanisms of complex chemical processes and its software implementation, Journal of Mathematical Chemistry, 51(1) (2013) 73–107.

[42] M. Musick, P.J. VanTiggelen, J. Vandooren, Experimental study of the structure of several fuel-rich premixed flames of methane, oxygen, and argon, Combust. Flame 105 (1996) 433–450.

[43] E. Ranzi, A. Sogaro, P. Gaffuri, G. Pennati, T. Faravelli, A wide range modeling study of methane oxidation, Combust. Sci. Technol. 96 (1994) 279–325.

[44] T. Kasper, P. Oßwald, U. Struckmeier, K. Kohse-Höinghaus, C.A. Taatjes, J. Wang, T.A. Cool, M.E. Law, A. Morel, P. R. Westmoreland, Combustion chemistry of the propanol isomers - investigated by electron ionization and VUV-photoionization molecular-beam mass spectrometry, Combust. Flame 156 (2009) 1181–1201.

[45] N. Faßheber, G. Friedrichs, P. Marshall, P. Glarborg, Glyoxal oxidation mechanism: Implications for the reactions HCO + O2 and OCHCHO + HO2, J. Phys. Chem. A, 119 (2015) 7305–7315.

[46] W.H. Green, J.W. Allen, A. Beat, R. Buesser, W. Ashcraft, G.J. Beran, C.A. Class, C. Gao, C.F. Goldsmith, M.R. Harper, A. Jalan, M. Keceli, G.R. Magoon, D.M. Matheu, S.S. Merchant, J.D. Mo, S. Petway, S. Raman, S. Sharma, J. Song, Y. Suleymanov, K.M.V. Geem, J. Wen, R.H. West, A. Wong, H.-W. Wong, P.E. Yelvington, N. Yee, J. Yu, RMG v4.0.1, http://rmg.sourceforge.net/, 2013.

[47] S.M. Aschmann, R. Atkinson, Kinetics of the gas-phase reactions of the oh radical with selected glycol ethers, glycols, and alcohols, Int. J. Chem. Kinet., 30, (1998) 533–540.

[48] H.L. Bethel, R. Atkinson, J. Arey, Kinetics and products of the reactions of selected diols with the OH radical, Int. J. Chem. Kinet., 33 (2001) 310–316.

SUPPLEMENTAL MATERIAL

to

Kinetics of Ethylene Glycol: The first validated reaction scheme and first measurements of ignition delay times and speciation data

Trupti Kathrotia, Clemens Naumann, Patrick Oßwald, Markus Köhler, Uwe Riedel*

Institute of Combustion Technology, German Aerospace Center (DLR), Pfaffenwaldring 38-40, D-70569 Stuttgart, Germany

1. Ethylene glycol model reduction and validation

The detailed reaction model of ethylene glycol discussed in the main paper including C_1-C_4 chemistry contains 78 species and 574 forward reactions. In order to model and understand complex chemical and physical process occurring inside gasifiers, one requires multi-dimensional CFD simulations. For its further use in CFD, this reaction mechanism is reduced in number of species and reactions. Modeling chemical process with detailed gas phase chemistry is useful in understanding the products and intermediates that are formed inside the system as well as insights into heat release can be obtained. For example, Large Eddy Simulation (LES) of multiphase reactive flow in the near-field of an entrained flow gasifier injector has been modeled by Eckel et al. [1-3]. Here, a reduced ethylene glycol mechanism has been used to model the gas-liquid phase. Such approaches provide insights into the species and temperature field as well as droplet dispersion.

In the present work, the reduction of detailed model was carried out with the target to keep the prediction of ignition delay time of EG as well as the prediction of intermediates and products as close to the detailed mechanism as possible.

For the reduction of the detailed mechanism to a reduced (skeletal) mechanism, the reaction mechanism reduction module of chemical workbench [4] was used. For the reduction procedure, we selected the Directed Relation Graph (DRG) method [5]. The global combustion characteristics, ignition delay times (for 1 and 16 bar) and atmospheric flame velocity both at Φ = 1.0 is supplied as reduction target. The aim of this work is not to

maximize reduction (minimize species) but to obtain a compact mechanism with still keeping the best prediction of not just global parameters only but also of intermediate species concentration profiles such as CO, CO_2, H_2O, H_2 etc. which are important products in gasification. Thus, a final reduced skeletal model containing 43 species and 270 reactions is obtained which is about 50% reduction of the detailed mechanism. The reduced model performs within an uncertainty of maximum 20% compared to the detailed model. Comparison of the reduced with the detailed model predictions are provided in the following section.

1.1 Ignition delay times

The ignition delay times are perfectly reproduced by the reduced model and the difference between predictions of the ignition delay times by the detailed and the reduced model are hardly visible. Figure S1 presents such a comparison.

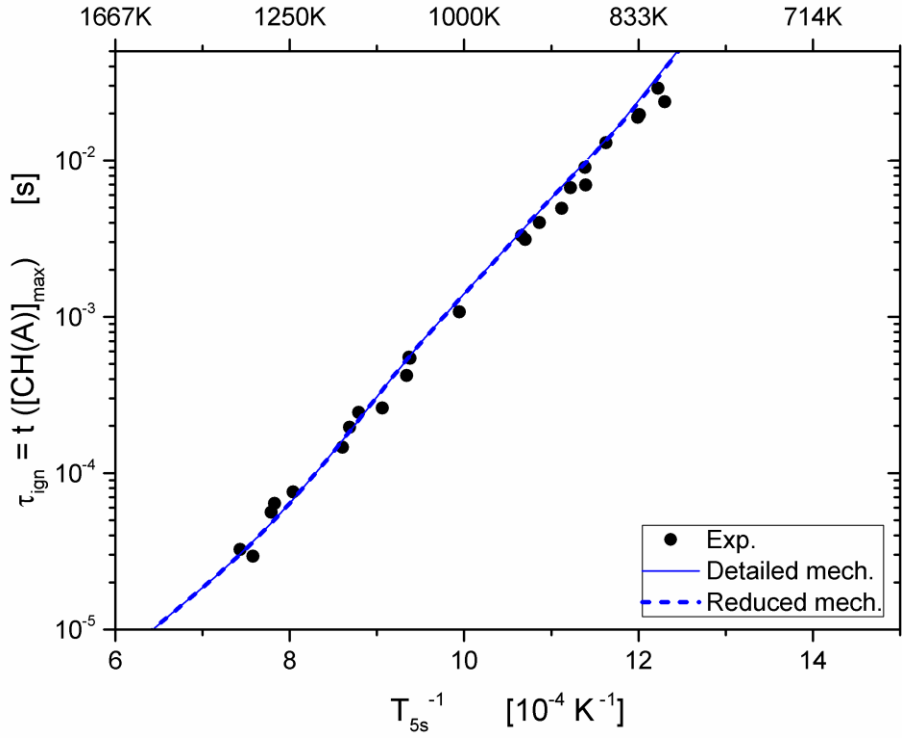

Fig. S1: Comparison of the reduced and the detailed model of Ethylene glycol – measured (symbols) and computed (lines) ignition delay times for a pressure of 16 bar in the temperature range of 800 – 1500 K for a stoichiometric fuel / synthetic air mixture at Φ = 1.0, diluted 1:2 in nitrogen. The synthetic air composition is 80% nitrogen and 20% oxygen. Reduced model: dashed line, detailed model: solid line.

1.2 Species profiles in flow reactor, Φ = 1.0

Figures S2 to S11 presents the predictions of flow reactor profiles by showing the reduced model in comparison to the detailed model. Among the species eliminated in the reduction procedure are C_3 – C_4 hydrocarbons which has nearly no influence on the EG chemistry. They may be important for very rich conditions where soot formation takes place. However, the present model does not include soot formation paths; therefore, they are not considered

important. All the reduced model species predictions presented in the following figures are very close to the detailed mechanism.

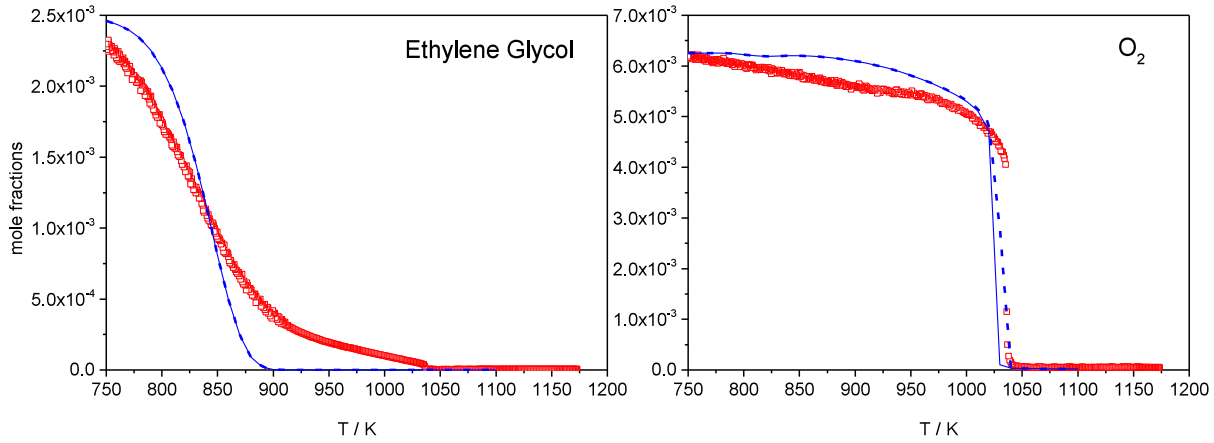

Fig. S2: Comparison of the reduced with the detailed reaction model. Mole fraction profiles of fuel and oxidizer as a function of the respective oven temperatures (T) for Φ = 1.0. Symbols represent experimental data and lines represent modeling results. Reduced model (dashed line), detailed model (solid line).

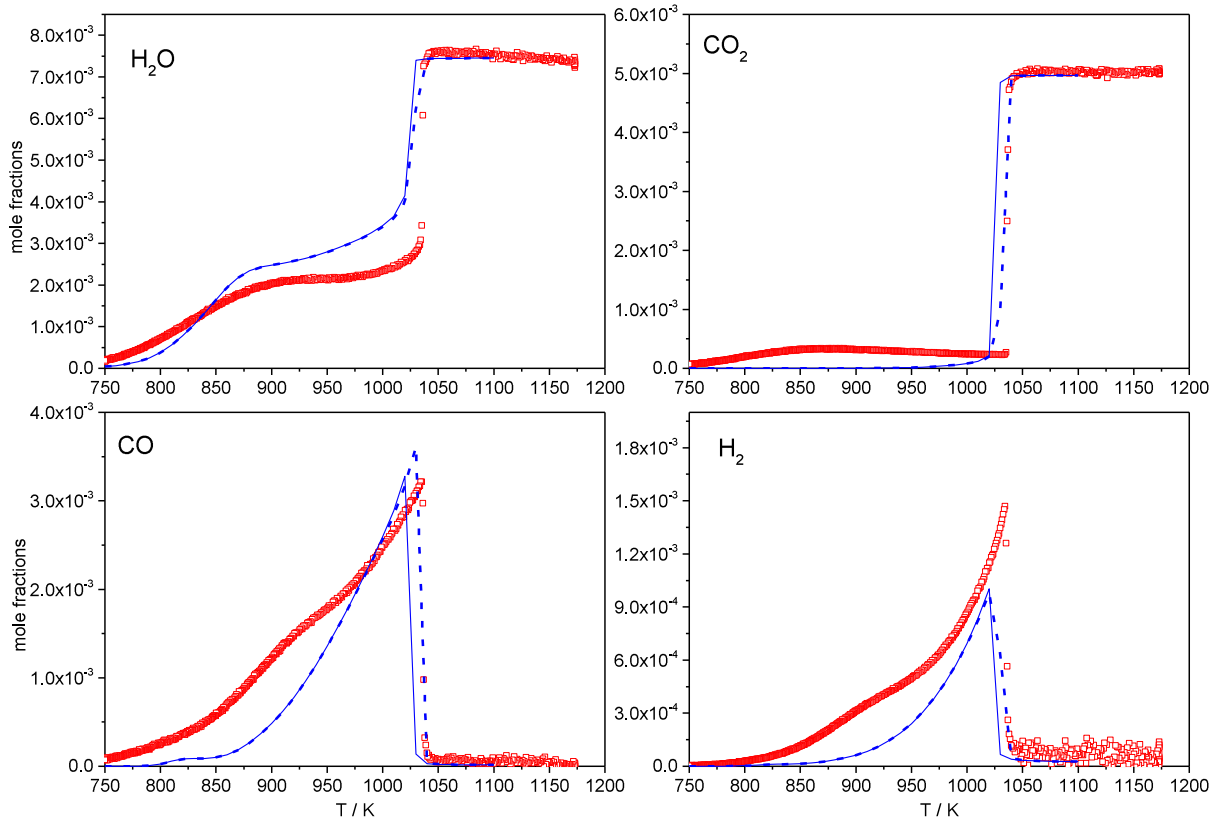

Fig. S3: Comparison of the reduced reaction model with the detailed model. Mole fraction profiles of major species CO, CO_2, H_2O, and H_2 as a function of the respective oven temperatures (T) for Φ = 1.0. Symbols represent experimental data and lines represent modeling results. Reduced model (dashed line), detailed model (solid line).

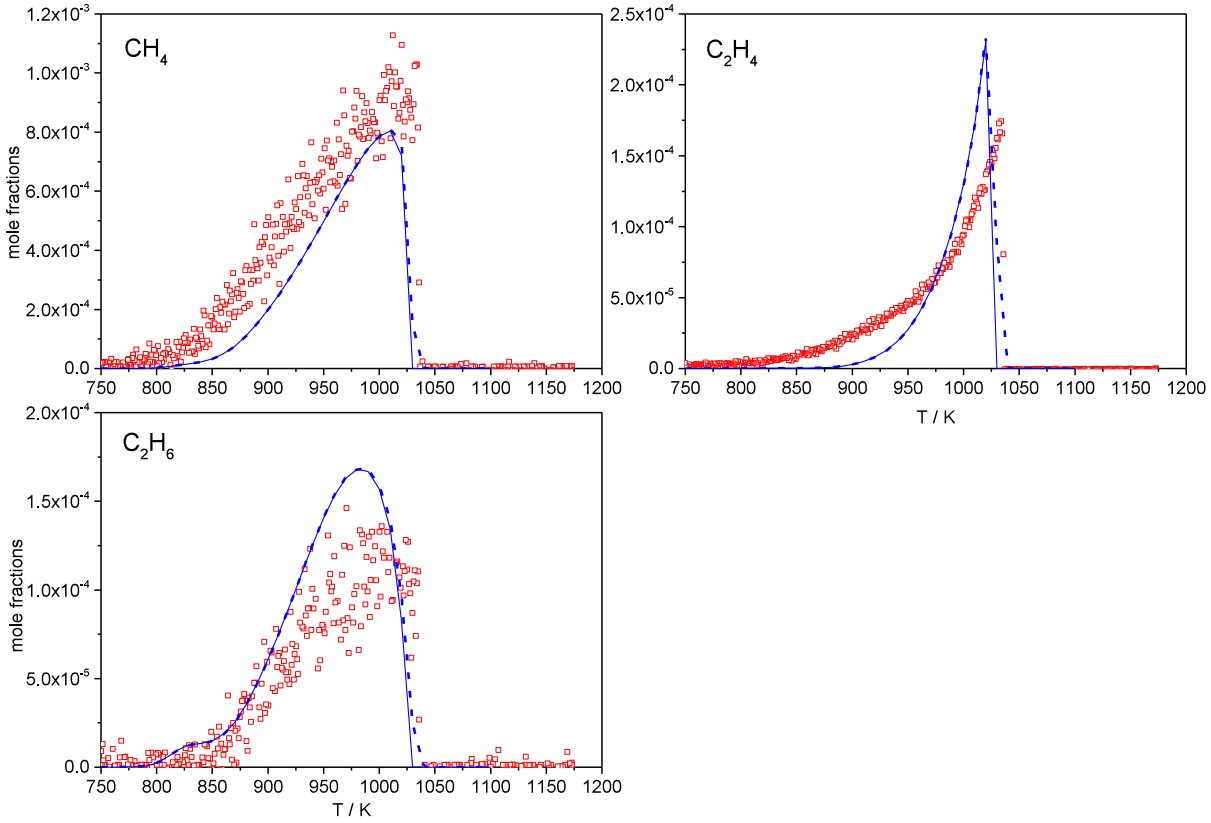

Fig. S4: Comparison of the reduced reaction model with the detailed model. Mole fraction profiles of hydrocarbon intermediates as a function of the respective oven temperatures (T) for Φ = 1.0. Symbols represent experimental data and lines represent modeling results. Reduced model (dashed line), detailed model (solid line).

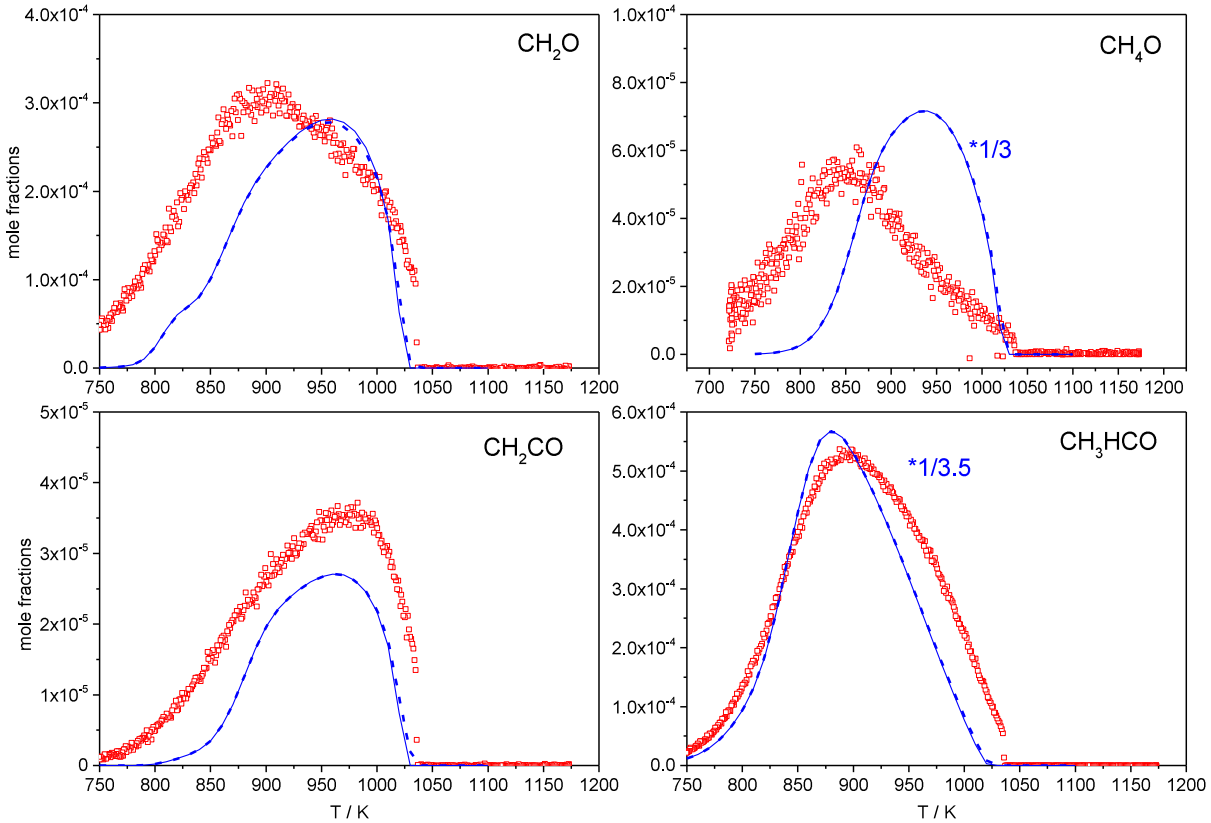

Fig. S5: Comparison of the reduced reaction model with the detailed model. Mole fraction profiles of

oxygenated intermediates as a function of the respective oven temperatures (T) for Φ = 1.0. Symbols represent experimental data and lines represent modeling results. Reduced model (dashed line), detailed model (solid line). To facilitate comparison of the respective trends, a scaling factor (model data scaled roughly to maximum experimental value) indicated when applied.

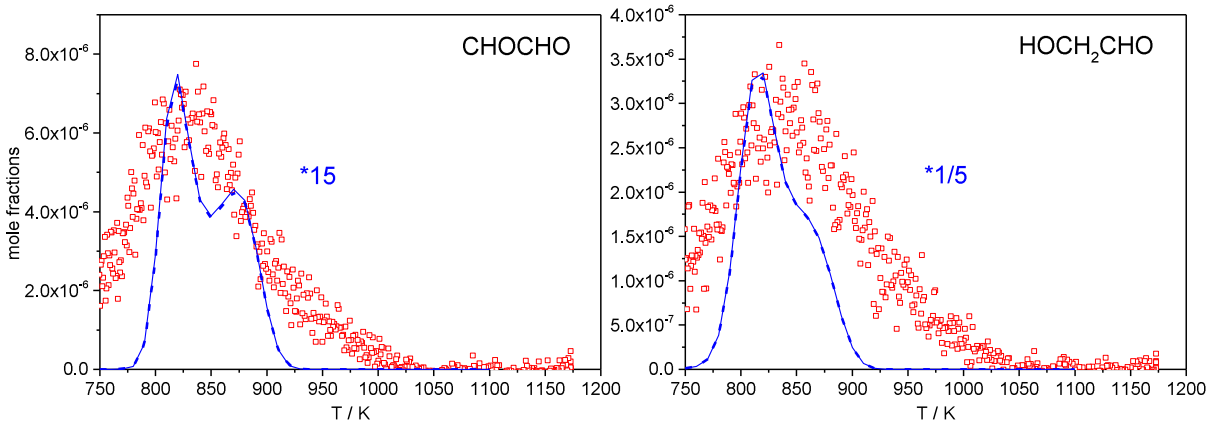

Fig. S6: Comparison of the reduced reaction model with the detailed model. Mole fraction profiles of di-oxygenated intermediates as a function of the respective oven temperatures (T) for Φ = 1.0. Symbols represent experimental data and lines represent modeling results. Reduced model (dashed line), detailed model (solid line). To facilitate comparison of the respective trends, a scaling factor (model data scaled roughly to maximum experimental value) indicated when applied.

1.3 Species profiles in flow reactor, Φ = 2.0

Species profiles comparison of detailed and reduced model for fuel rich mixture (Φ = 2.0) are presented in following figures. As with the stoichiometric case, the profiles of reduced model for fuel-rich case are equally capable to well reproduce the experimental profile.

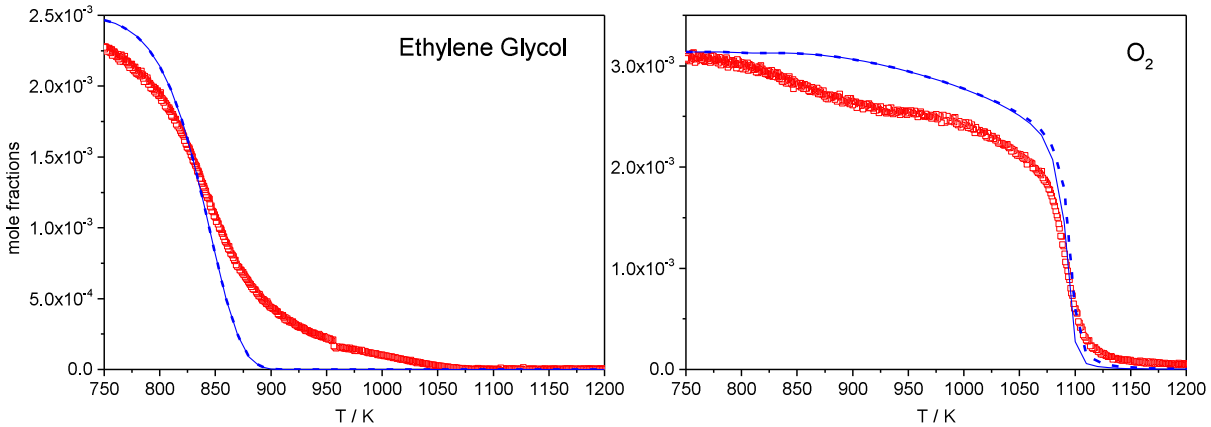

Fig. S7: Comparison of the reduced reaction model with the detailed model. Mole fraction profiles of fuel and oxidizer as a function of the respective oven temperatures (T) for Φ = 2.0. Symbols represent experimental data and lines represent modeling results. Reduced model (dashed line), detailed model (solid line).

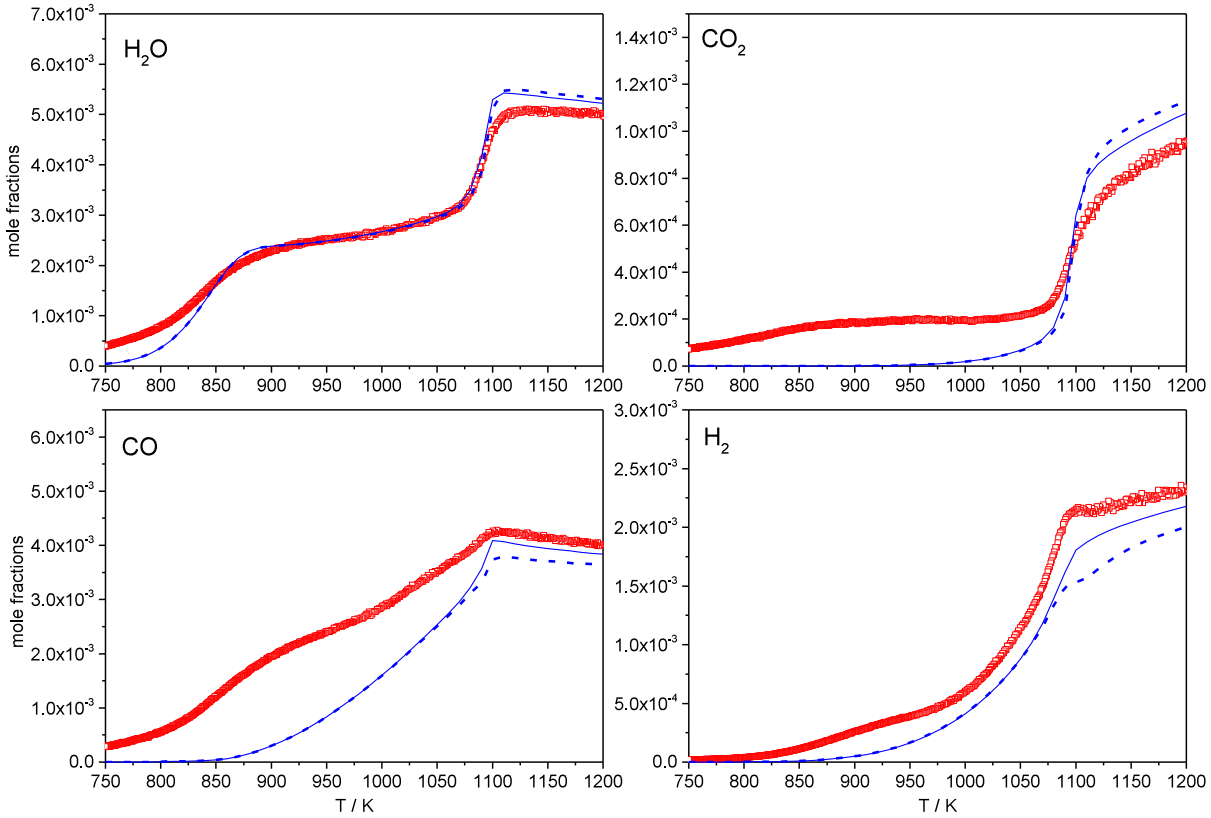

Fig. S8: Comparison of the reduced reaction model with the detailed model. Mole fraction profiles of major species CO, CO_2, H_2O, and H_2 as a function of the respective oven temperatures (T) for Φ = 2.0. Symbols represent experimental data and lines represent modeling results. Reduced model (dashed line), detailed model (solid line).

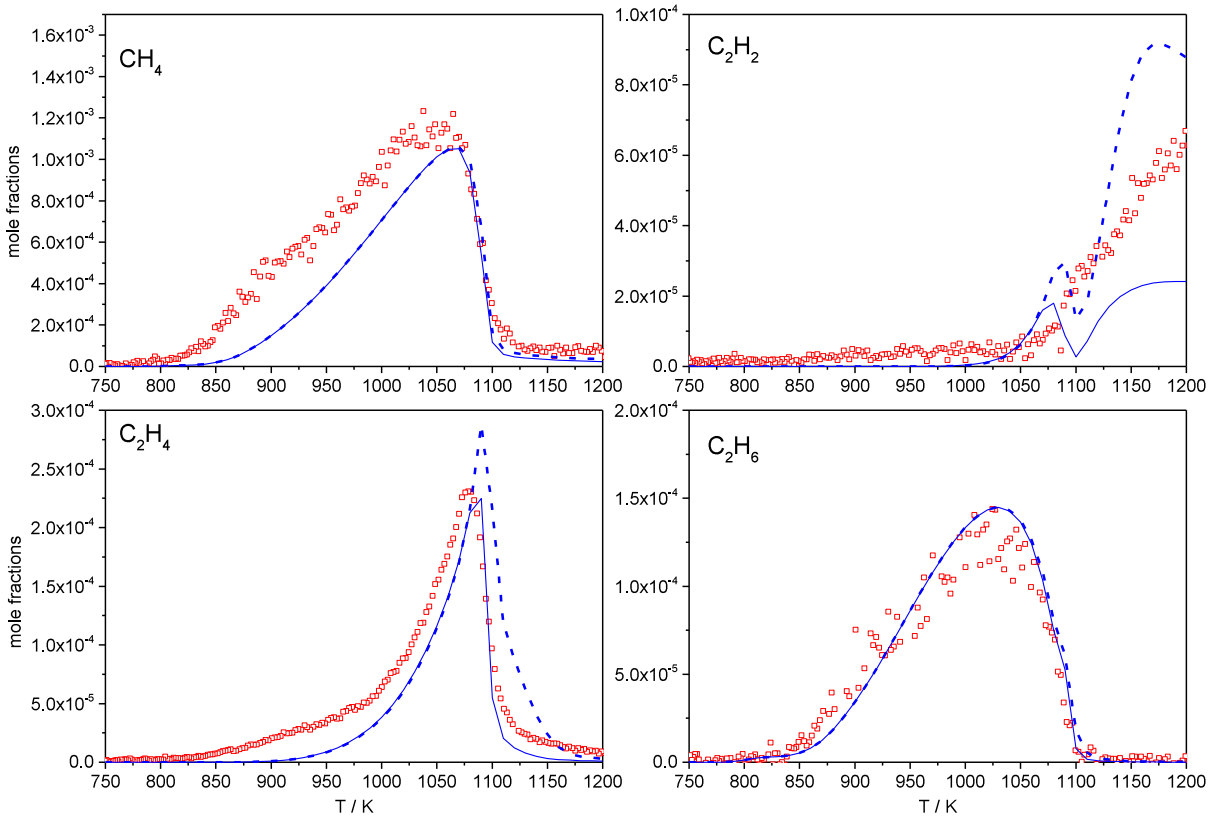

Fig. S9: Comparison of the reduced reaction model with the detailed model. Mole fraction profiles of hydrocarbon intermediates as a function of the respective oven temperatures (T) for Φ = 2.0. Symbols

represent experimental data and lines represent modeling results. Reduced model (dashed line), detailed model (solid line).

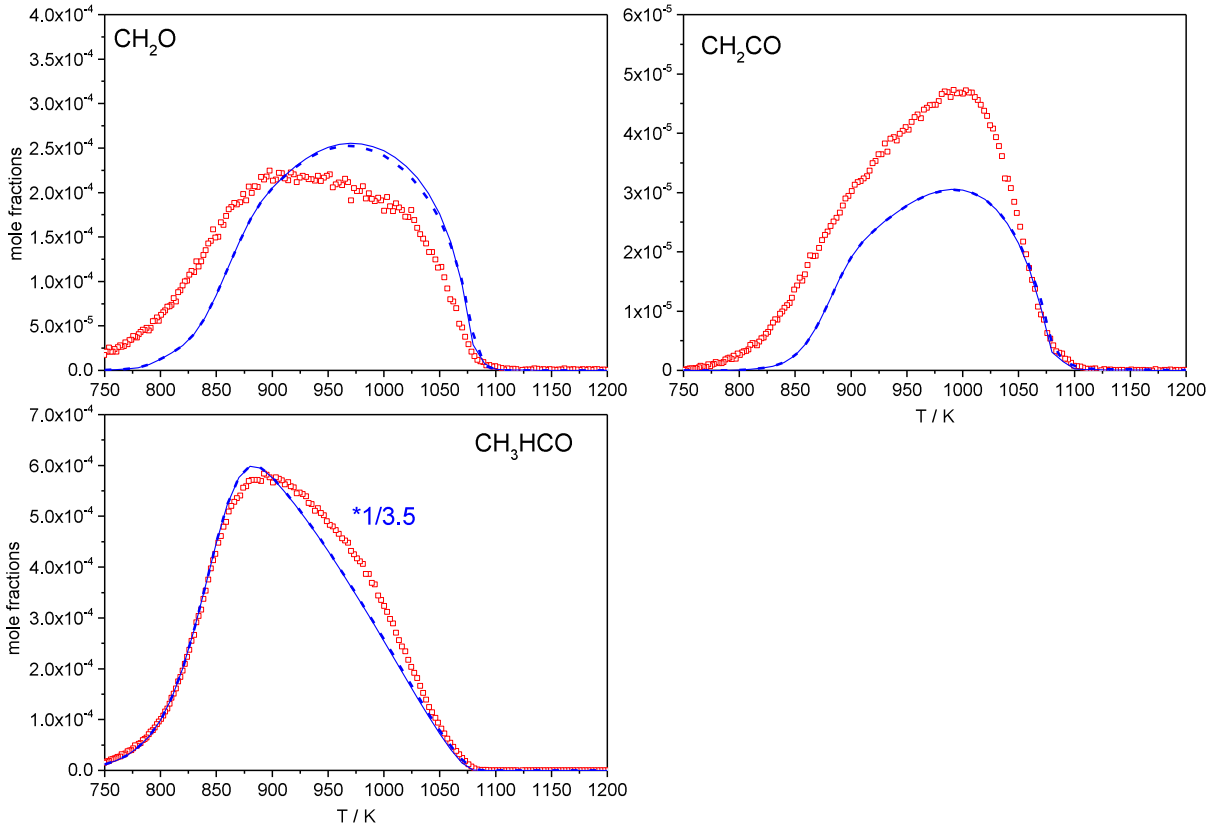

Fig. S10: Comparison of the reduced with the detailed model. Mole fraction profiles of oxygenated intermediates as a function of the respective oven temperatures (T) for Φ = 2.0. Symbols represent experimental data and lines represent modeling results. Reduced model (dashed line), detailed model (solid line). To facilitate comparison of the respective trends, a scaling factor (model data scaled roughly to maximum experimental value) indicated when applied.

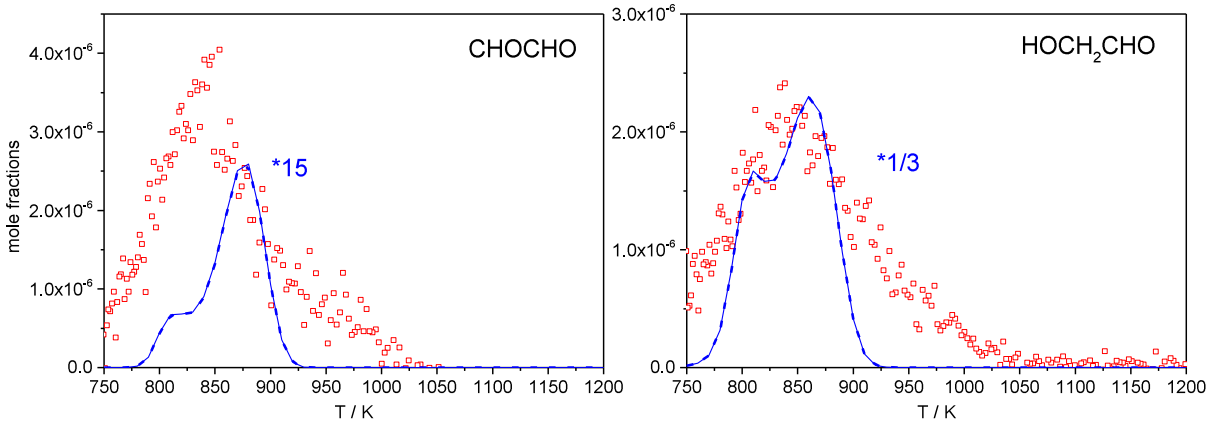

Fig. S11: Comparison of the reduced with the detailed model. Mole fraction profiles of di-oxygenated intermediates as a function of the respective oven temperatures (T) for Φ = 2.0. Symbols represent experimental data and lines represent modeling results. Reduced model (dashed line), detailed model (solid line). To facilitate comparison of the respective trends, a scaling factor (model data scaled roughly to maximum experimental value) indicated when applied.

2. Experimental setup

The Figures S12 and S13 shows schematic of shock-tube setup.

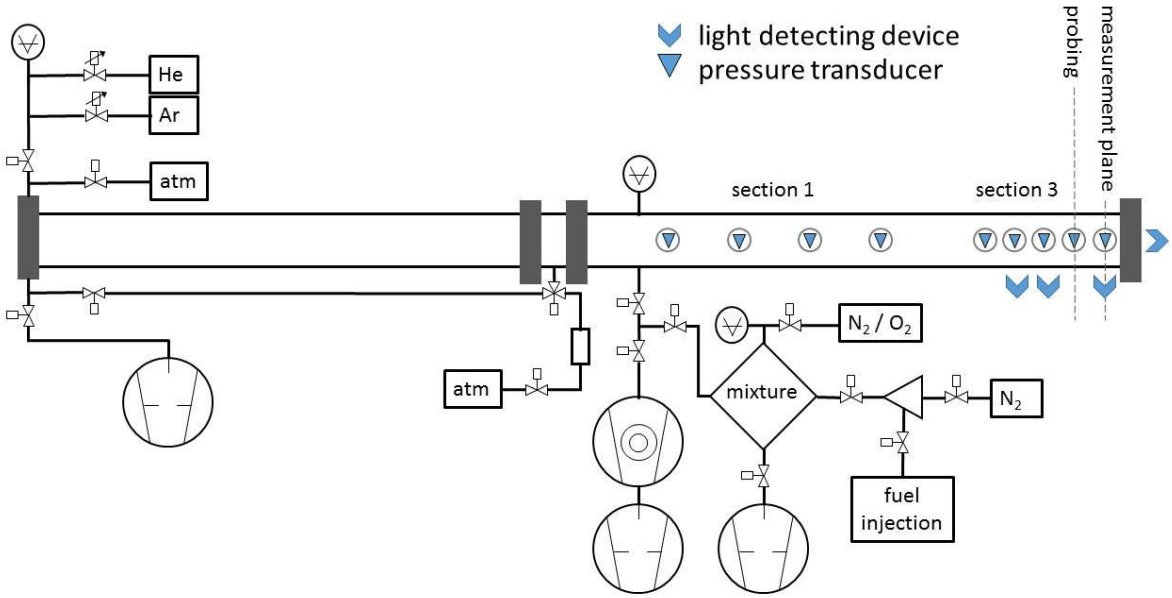

Fig. S12: High pressure shock tube (driver / intermediate volume / driven)

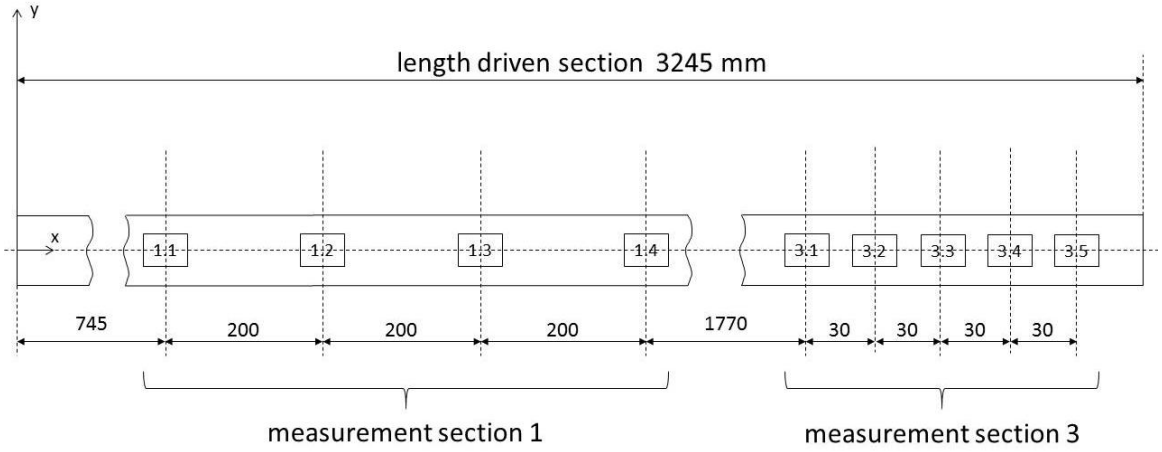

Fig. S13: High pressure shock tube (driven section): Measurement sections #1 and #3. Relevant instrumentation: All measurement planes are equipped with one pressure transducer (PCB or KISTLER) at least. The end plate, following plane 3.5, and the measurement planes 3.2, 3.3 and 3.5, are equipped with windows for CH*-emission detection. Probing port is located at measurement plane 3.4

A schematic of the reactor setup is shown in Fig. S14 [6]. The system consists of the high temperature reactor, including the gas supplies and the coupled gas analyzer i.e. a molecular beam mass spectrometry (MBMS) system.

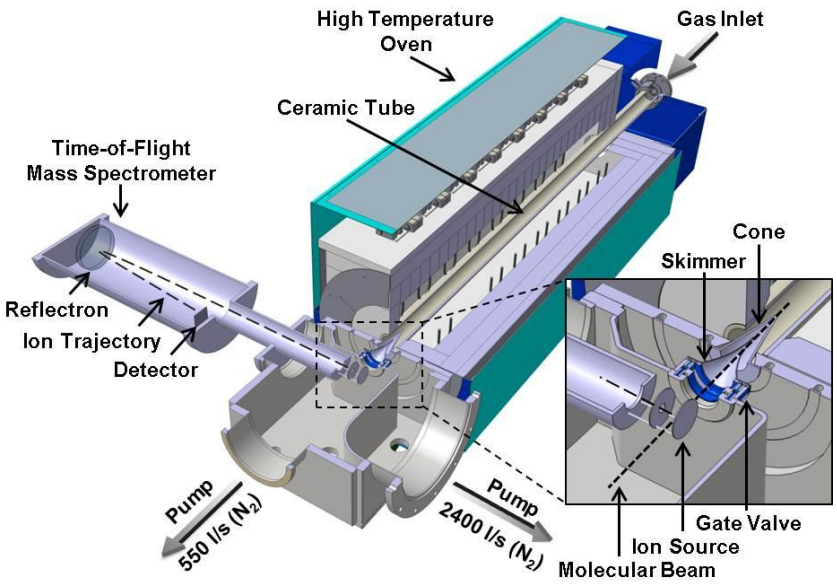

Fig. S14: Schematic of the flow reactor and mass spectrometer from [6].

References:

[1] G. Eckel, A. Saenger, C. Hotz, T. Kathrotia, M. Rachner, P. Le Clercq, M. Aigner, LES of a reactive, multi-phase flow in the injector near-field of an entrained-flow gasifier, International Conference on Multiphase Flow, Firenze, Italy, May 22 - 27, 2016.

[2] T. Kolb, M. Aigner, R. Kneer, M. Mueller, R. Weber, N. Djordjevic, J. Energ. Inst., 89 (2016) pp. 485-503.

[3] U. Santo, H. Seifert, T. Kolb, L. Krebs, D. Kuhn, H. Wiemer, E. Pantouflas, N. Zarzalis, Chem. Eng. Technol., 30(7) (2007) pp. 967–969.

[4] Chemical WorkBench® 4.0, Kintech Lab. (2013) http://www.kintechlab.com/products/chemical-workbench/.

[5] A. V. Lebedev, M. V. Okun, V. A. Chorkov, P. M. Tokar. M. Strelkova, Journal of Mathematical Chemistry, 2013, 51(1), pp. 73–107, DOI 10.1007/s10910-012-0065-z.

[6] P. Oßwald, M. Köhler, Rev. Sci. Instrum. 86 (10) (2015), pp. 105109, doi: 10.1063/1.4932608.